

CO₂ degassing in the Hartoušov mofette area, western Eger Rift, imaged by CO₂ mapping and geoelectrical and gravity surveys

Tobias Nickschick · Horst Kämpf · Christina Flechsig ·
Jan Mrlna · Jens Heinicke

Received: 9 April 2014 / Accepted: 28 December 2014 / Published online: 13 January 2015
© Springer-Verlag Berlin Heidelberg 2015

Abstract Strong, subcontinental mantle-dominated CO₂ degassing occurs in the Hartoušov and Bublák mofette fields in the western Eger Rift. The combination of CO₂ gas flux and soil gas measurements as well as gravity and geoelectric surveys provides insight into the surface and subsurface of this unique mofette area. CO₂ soil gas and gas flux measurements reveal that large amounts of carbon dioxide are released via channels with diameters below 1 m. Carbon dioxide emissions of several tens and up to more than 100 kg day⁻¹ are ejected via these small seeps. Measurements with small spacings are necessary to account for the point like, focused gas discharge in the lesser degassing surrounding. We estimate that between 23 and 97 tons of CO₂ are released over an area of about 350,000 m² each day in the Hartoušov mofette field. The application of widely used geostatistical tools leads to estimations of the CO₂ discharge with very high standard deviations due to the strong positive skewness of the data distribution. Geophysical investigations via electrical resistivity tomography and gravity measurements were carried out over areas of strong seepage and reveal distinct anomalies in the subsurface below mofettes, indicating rock and sediment alterations and/or sediment transport by pressurised, ascending CO₂ and water mobilised by it. This study reveals that the

gas emanations only occur west of a morphological step which is related to a N–S-oriented fault zone, the Počatky-Plesná fault zone. The results of CO₂ mapping and the geo-physical studies can track the course of this fault zone in this area. Our results fit into a tectonic model in which the mofette fields are in the centres of two independent pull-apart basin-like structures. We hypothesise that the sinistral strike-slip movement of the Počatky-Plesná fault zone leads to a pull-apart basin-like opening, at which the strong, mantle-derived CO₂ degassing occurs nowadays. Since the Hartoušov and Bublák mofette fields only illustrate examples along the N–S-striking Počatky-Plesná fault zone, its role and other N–S-striking faults' roles of the Regensburg–Leipzig–Rostock zone for upper mantle degassing might have been underestimated previously.

Keywords Cheb Basin · Magmatic CO₂ · Eger Rift · CO₂ gas flux studies · Geoelectrics · Gravity

Introduction

The West Bohemia/Vogtland region is the geodynamically most active area near the European Cenozoic Rift showing persistent seismic activity in the form of recurring earthquake swarms and intense CO₂-degassing at the surface with mantle-derived He-isotope signatures. These intra-plate earthquake swarms are characterised by magnitudes up to ML 4.5 and focal depths between 4 and 20 km (Horálek and Fischer 2010). The area is known as “locus typicus” for the term “earthquake swarm”, established by Credner, more than 100 years ago (Credner 1876). Historical data document earthquake activity even since the twelfth century in Bohemia (Kárník et al. 1957) and since the sixteenth century in Saxony (Grünthal 1989). The epicentres are not equally

T. Nickschick (✉) · H. Kämpf
German Research Centre for Geosciences GFZ Potsdam,
Section 4.3 Telegrafenberg, 14473 Potsdam, Germany
e-mail: tnickschick@gmx.de

C. Flechsig · J. Heinicke
University Leipzig, Institute for Geophysics and Geology,
Talstraße 35, 04103 Leipzig, Germany

J. Mrlna
Czech Academy of Sciences, Institute of Geophysics,
Bocni II 1401, 14131 Prague, Czech Republic

distributed over the study region, but are concentrated in some clusters in the Southern Vogtland, the Fichtelgebirge/Oberpfalz and the area of the Cheb Basin and Slavkovský Les (Neuhöfer and Hemmann 2005; Horálek and Fischer 2010; Fischer et al. 2014). Most of the earthquake activity is concentrated at the Nový Kostel focal zone (NKFZ), located at the intersection between the N–S-trending Počátky-Plesná Fault Zone (PPZ) and the NW-trending Mariánské Lázně Fault Zone (MLFZ) (Fischer 2003; Fischer et al. 2012, 2014). About 90 % of the total seismic moment was released in the NKFZ, which was formed by an NNW-striking and steeply dipping fault plane (Horálek and Fischer 2010). Alexandrakis et al. (2014) investigated the v_p/v_s ratio of the NKFZ and its surrounding by double-difference tomography. They found structures that may reflect changes in the lithology and/or fluid concentration in the hypocentral area and that an overlaying body of granitic intrusion acts as a fluid trap. Swarm-like seismic activity near Nový Kostel was recorded in 1985/1986, 1997, 2000, 2008, 2011–2012 (Fischer et al. 2014) and in 2014 (ML = 4.5).¹

Results of seismological investigations prove that the structure of the lithosphere of this area is anomalous compared to the surroundings. The results were interpreted as crustal thinning to about 27 km (Geissler et al. 2005; Heuer et al. 2006). Hrubcová and Geissler (2009) found a ca. 5-km-thick layer in the lower crust (Moho reflective zone), while Hrubcová et al. (2013) found out that the thickness of the Moho reflective zone varied between 2 and 4 km within depth range of 27/28–31.5 km. Heuer et al. (2006) detected a zone of lower velocity at ca. 65 km depth which was interpreted as asthenospheric up-doming and/or may be caused by the occurrence of partial melt. Heuer et al. (2011) assumed a small plume structure with only weak imprint on the 410 km discontinuity beneath this area.

Most earthquake swarms in rifting regimes are related to magmatic dike intrusion or fluid transport processes in crustal faults. Earthquake swarms often form vertically oriented, planar shapes tracing the outline of the dike or fault, e.g. in Iceland (Jakobsdóttir et al. 2008; Key et al. 2011; White et al. 2011), in the western Eger Rift (ER), Central Europe (Bräuer et al. 2003; Dahm et al. 2008; Horálek and Fischer 2008; Fischer et al. 2014) and in Western Saxony SW of Zwickau, Central Europe (Hemmann and Kämpf 2002; Hemmann et al. 2003; Korn et al. 2008), Afar (Ebinger et al. 2008), the southern Kenya Rift (Ibs-von Seht et al. 2001) or the Long Valley Caldera, California/USA (Hill and Prejean 2005).

Weinlich et al. (1998, 1999, 2003) and Kämpf et al. (2007) carried out initial mappings of the gas and isotope

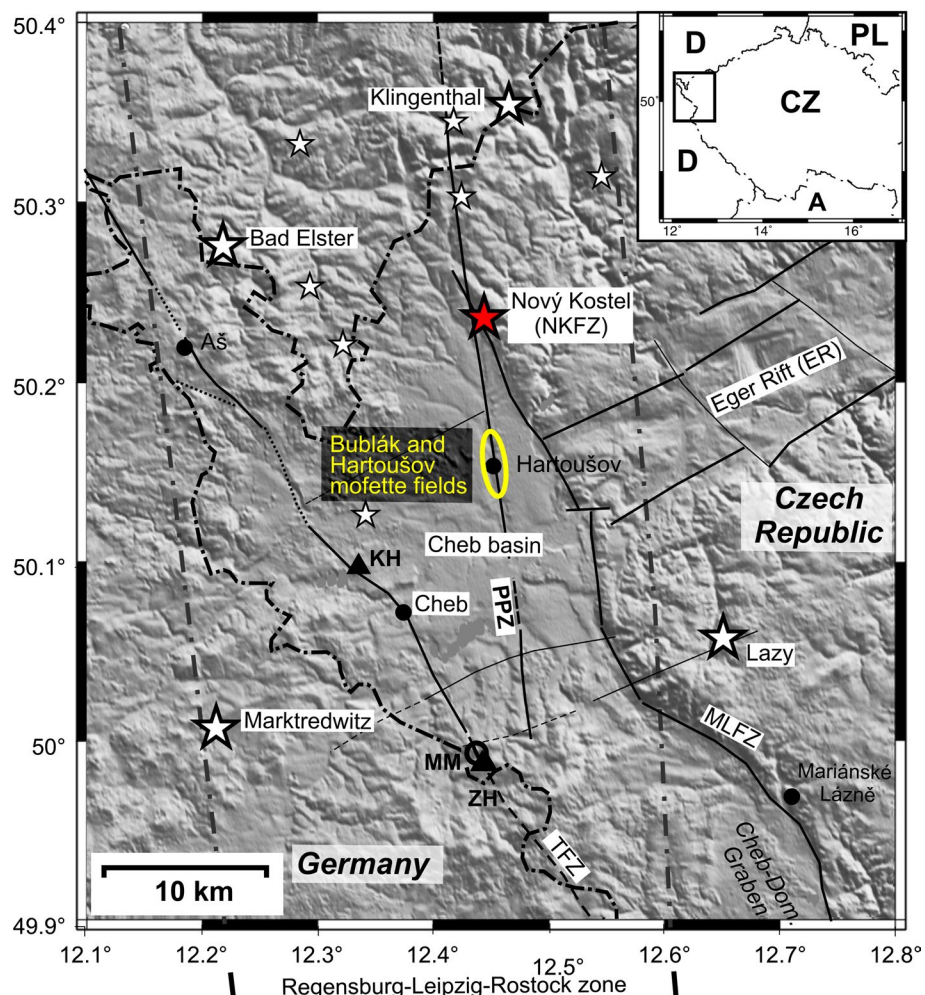
($^3\text{He}/^4\text{He}$, $\delta^{13}\text{C}_{\text{CO}_2}$) composition of free gas at mofettes and mineral springs in the western ER and provided a first estimation of the vent-bound CO_2 emission rate. Three different degassing centres could be distinguished in the region: Karlovy Vary, Mariánské Lázně and surroundings, and the Tertiary Cheb Basin. They showed a similar $\delta^{13}\text{C}_{\text{CO}_2}$ signature between –4 and –2 ‰, but different levels of mantle-derived helium: Karlovy Vary (≈ 2.4 Ra), Mariánské Lázně (≈ 4.6 Ra) and Cheb Basin (≈ 6 Ra), which covers the range of the subcontinental lithospheric mantle (SCLM) according to Gautheron et al. (2005). $^3\text{He}/^4\text{He} > 6$ Ra reflects a high percentage of mantle-derived helium and little mixing with helium from the crust (Bräuer et al. 2008). Several time series of gas isotope measurements of N, He and C indicated that an active hidden magmatic process has been ongoing since ca. 2000 beneath the eastern part of the Cheb Basin (Bräuer et al. 2005, 2008, 2009, 2011, 2014; Fischer et al. 2014). The increase in mantle-derived helium is both temporally and spatially progressive. Increases were first observed at the Bublák mofette field (BMF), then at Hartoušov, which is just about 1.5 km south of Bublák, along the PPZ, and subsequently along the MLFZ at Dolní Častkov (Bräuer et al. 2009). In addition, a 3-month-lasting increase of mantle-derived helium up to 6.3 Ra was observed at the Bublák mofette in March–May 2006. From the high gas flux and high $^3\text{He}/^4\text{He}$ ratios (covering the SCLM range), the mofette fields surrounding Bublák and Hartoušov appear to act as deep-seated fluid migration zones along the PPZ (Bräuer et al. 2011). The distinct increase in the $^3\text{He}/^4\text{He}$ ratios over a 3-month period at the monitoring locations was interpreted as an indication of a dike intrusion with fresh magma from the deeper reservoir probably located in the lithospheric mantle at ca. 65 km depth (Bräuer et al. 2009, 2011). Geissler et al. (2005) argue that all these observations are somehow interrelated by an active zone of mantle melting and magmatic underplating associated with recent extensional tectonics.

One of the open questions regarding the understanding of geodynamics—especially triggering mechanisms of earthquake swarms—is a profound knowledge of the magma intrusion/fluid migration in the earth's lithosphere via dikes, conduits or faults (Caine et al. 1996). However, since the terrestrial CO_2 conduits—unlike their marine hydrocarbon counterparts (Loseeth et al. 2009)—are hard to detect by seismic profiling, information on the evolution, geometry—including permeability—and the constancy of the small-scale, terrestrial degassing structures in space and time is scarce.

According to the results of former investigations (Flechsig et al. 2008; Kämpf et al. 2013), this degassing area represents an excellent example for studying the relationship between the emission of fluids from the lithospheric mantle and near-surface structural and lithological controls. In

¹ <http://www.ig.cas.cz/en/structure/observatories/west-bohemia-seismic-network-webnet/earthquakes-west-bohemia-2014>. Access on June 2nd, 2014.

Fig. 1 Schematic map with main fault zones, Quaternary volcanoes and the location of the survey site in the western Eger Rift zone (yellow ellipse). MLFZ Mariánské Lázně fault zone, PPZ Počátky-Plesná fault zone, TFZ Tachov fault zone, ZH Železná hůrka scoria cone, MM Mýtina maar, KH Komorní hůrka scoria cone. Large white stars mark the most active earthquake swarm areas, smaller ones mark areas with less activity. Modified after Ibs-von Seht et al. (2008), Mrlna et al. (2009), Horálek and Fischer (2010), Fischer et al. (2014)



order to extend the geophysical investigation in the CO₂ degassing and fault zone area and to correlate the subsurface information to the CO₂ study, a combination of resistivity surveys and microgravity measurements was chosen. Multidisciplinary approaches of combined gas studies and geophysical surveys have been carried out mainly in volcanically active areas (Carapezza et al. 2009; Finizola et al. 2006, 2009, 2010; Revil et al. 2008, 2011). Integrated studies are also known in case of degassing structures caused by thermometamorphic alteration of carbonate units (Arts et al. 2009; Pettinelli et al. 2008, 2010). Byrdina et al. (2009) have applied CO₂, radon, SP mapping, as well as ERT measurements in a non-volcanic area in a tectonically active zone in central Nepal, characterised by an intense microseismicity and deep CO₂ emissions. Thus, the application and combination of different geological, geochemical and geophysical methods are well suited in the research of diffuse degassing structures (DDS, Chiodini et al. (2001)).

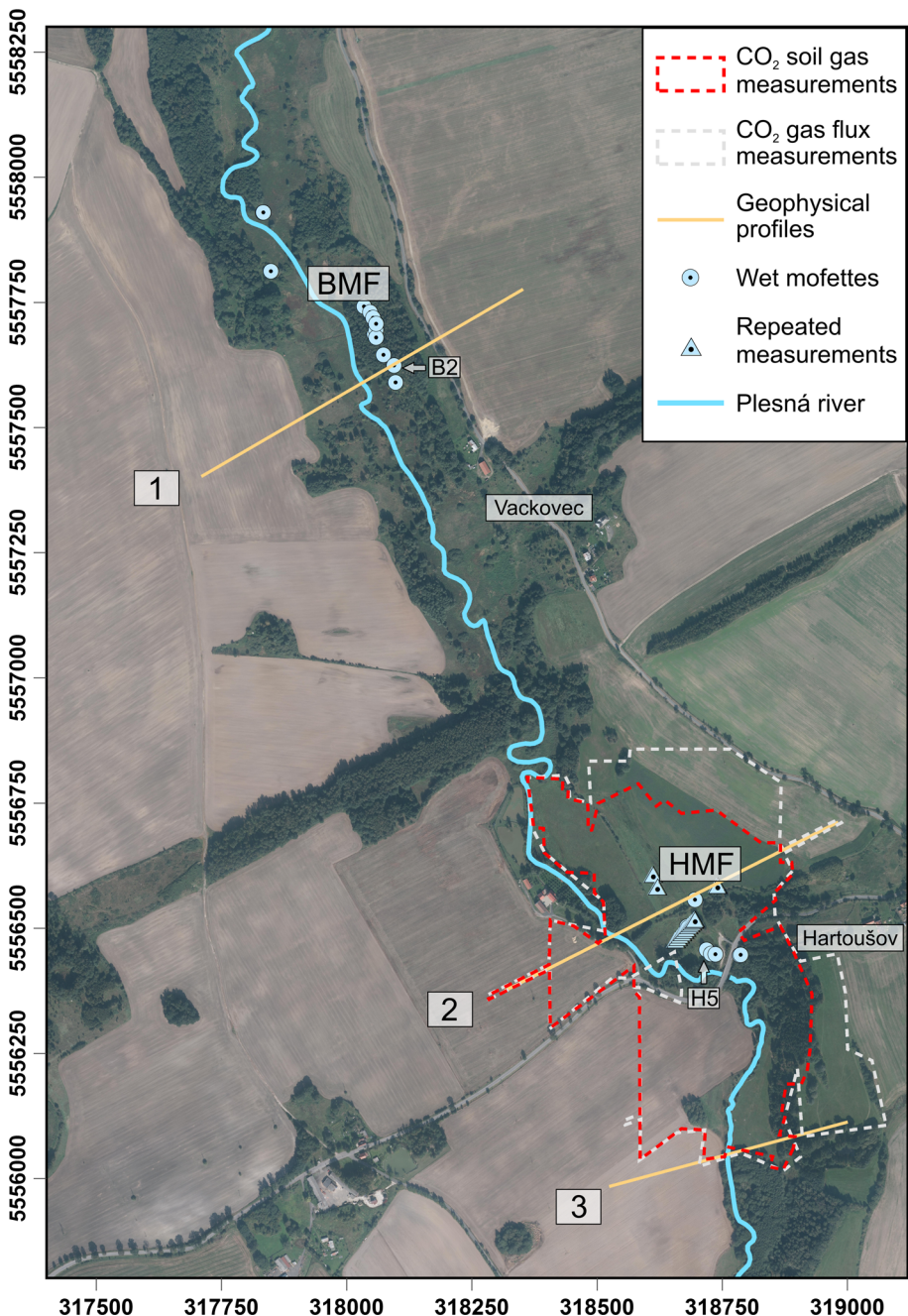
Based on preliminary investigations of Flechsig et al. (2008) and Kämpf et al. (2013), the aim of the presented study was to localise and quantify the mantle-derived

CO₂ emission and to evaluate the geological and tectonic background of the gas pathways inside diffuse degassing structures using different geoscientific methods, such as CO₂ soil gas and gas flow measurements, electric resistivity tomography and gravimetry. This combination provides a meaningful approach in the observation of near-surface fluid transport and migration ways, useful for the detection and monitoring along active faults.

Geological and geophysical setting

The area under investigation is located in the northeastern Cheb Basin (Fig. 1, inset map) in the Bohemian Massif. There, the dominating rocks are rock sequences from Upper Cambrian to Ordovician age and areas with Late Variscan intrusions dominated by granites. The Cheb Basin is a small intra-continental basin and lies within the western part of the ER. The crystalline basement of the Cheb Basin consists of muscovite granites of the Smrčiny/Fichtelgebirge Pluton (Hecht et al. 1997) and

Fig. 2 Aerial view of the study area with locations of CO_2 soil gas, CO_2 gas flux, geoelectrical and gravimetric surveys. BMF is the Blublák mofette field, HMF is the Hartoušov mofette field. B2 and H5 are isotope sample locations (see inset in Fig. 10). All coordinates in WGS84/UTM zone 33



crystalline schists of the Saxothuringian Zone of the Variscan Orogen (muscovite–biotite mica-schists of phyllitic appearance) (Fiala and Vejnar 2004). The Cheb Basin, located in the intersection of the ENE-trending ER and the N–S-trending Regensburg–Leipzig–Rostock Zone (RLRZ, Fig. 1), was formed during the Late Tertiary and Quaternary as a result of the reactivation of Hercynian faults and/or separated microplates, present within the basement (Bankwitz et al. 2003b; Mlčoch 2003; Babuška and Plomerová 2008). The NW-trending pre-Neogene

MLFZ forms the eastern boundary of the Cheb Basin and is marked by a 50- to 100-m-high escarpment that can be traced along strike for over 100 km. The basin was filled with fluvial and lacustrine sediments (≤ 300 m thick) (Špicáková et al. 2000; Mlčoch and Skácelová 2009; Rojík et al. 2010).

Locally, Eocene clastics were first deposited and followed by Oligocene–Middle Miocene volcanoclastics, sands, clays and lignites. After a period of erosion in the Late Pliocene fluvial gravel, sand and kaolinitic clay

were deposited followed by Pleistocene sand and gravel. Holocene sand, silt and peat were the prevailing deposits in river valleys (Malkovský 1987; Špicáková et al. 2000; Flechsig et al. 2008, 2010; Rojík et al. 2010). The investigation area, the Hartoušov mofette field (HMF), is located in the flood plain of the Plesná river, at the eastern part of the Cheb Basin. HMF stretches approximately 500 m in NW direction and 350 m in NNW direction, (Fig. 2, all coordinates in the article are WGS84/UTM zone 33). According to Flechsig et al. (2008), the uppermost sediment units in the central part of HMF up to 10 m depth can be subdivided into three lithological units: (1) a basal fine-grained unit consisting predominantly of clay, silty clay and silt (age: Pliocene, thickness: >3 m), overlain by (2) a coarse-grained unit with sharp grain-size contrast dominated by sand and gravel (age: Pleistocene, thickness: ≈3–>4.5 m) and (3) an uppermost, rather heterogeneous unit, consisting of clay, silt, sand and peat (age: Holocene, thickness: 2–3.6 m).

According to Ulrych (2011) and Krüger et al. (2013), three periods of volcanic activity, including maar-diatreme volcanism for the northern and western part of the Bohemian Massif, can be defined: (1) pre-rift period (Later Cretaceous to Mid Eocene, 79–49 Ma), (2) syn-rift period (Mid Eocene to Mid Miocene, 42–16 Ma) and (3) late-rift period (16–0.26 Ma). At the Quaternary volcanic centres close to the Cheb Basin (see Fig. 1), two main stages of volcanic activity are recognised: explosive, phreatomagmatic initial stage and eruptive final stage with lava fountains and lava flows. Age determinations using different methods indicate that the Quaternary volcanic activities occurred in the Mid Pleistocene 0.78–0.12 Ma ago (Mrlna et al. 2009). $^{230}\text{Th}/^{234}\text{U}$ determinations of Karlovy Vary travertine deposits cover a wide time span ranging between 0.23 Ma BP and the present (Vylita et al. 2007) and give evidence that magmatic CO₂ escape dates back to about 0.23 Ma (Fischer et al. 2014).

As a first local comparative geoelectric, soil gas and sedimentological study of a magmatic CO₂ degassing vent in the Hartoušov mofette field, near-surface structures had been investigated by Flechsig et al. (2008). The investigations reveal structural and substantial features that are thought to be directly or indirectly related to CO₂ flow (anomalies of electrical resistivity and self-potential, sediment properties). In the same area Schütze et al. (2012, 2013), Sauer et al. (2013) and Sandig et al. (2014) tested several diagnostic monitoring tools at different scales to monitor processes taking place during CO₂ migration and seepage. Flechsig et al. (2010) also featured the application of geoelectric methods along the PPZ at “U Mostku”, just a few kilometres to the north of the Hartoušov mofette area and across the assumed course of the MLFZ to identify characteristic features of these faults.

Methods

CO₂ gas flux and CO₂ soil gas concentration

Field measurements

In the HMF, detailed mappings of the CO₂ content in the soil and the CO₂ gas flux at the surface were carried out to define the extent of diffuse degassing structures (Chiodini et al. 2001) and the amount of ejected CO₂ in soil gas. These methods have been successfully used in other volcanically and non-volcanically active areas, such as Bergfeld et al. (2001), Chiodini and Frondini (2001), Chiodini et al. (2010), Finizola et al. (2006, 2009), Lewicki et al. (2012), Schütze et al. (2012). The database used in this article comprises 3,003 measurements of the CO₂ content in the soil gas over an area of 310,000 m² and 3,770 measurements of the CO₂ gas flux [including the database of Kämpf et al. (2013)] over an area of 352,000 m². The CO₂ gas fluxes (762 measurements) and contents in soil (682 measurements) from Kämpf et al. (2013) were measured between 2007 and 2008, while the other measurements were carried out in 2009 and between 2012 and 2013. In all three field campaigns, measurements were carried out between April and October.

Measurements of the content of CO₂ soil gas were performed with an infrared gas analyser BM2000 (Ansyo/ Germany) at depths of 0.6–0.8 m in order to avoid atmospheric influence. Saßmannshausen (2010) and Rennert et al. (2011, Tab.1) show that the partial pressure of CO₂ can significantly change from the surface to 0.6 m depth. In dry summer seasons, it was possible to perform measurements at these depths most of the time even in areas where the ground water level is high during rainy seasons. The BM2000 gas analyser's accuracy is 0.5 % for up to 5 % CO₂, 1.0 % between 5 and 15 % CO₂ and 3 % for more than 15 % CO₂, as given by the manufacturer. However, we experienced larger variations in our measurements after carrying out additional repeated measurements at the same spot. This is in agreement with the findings of Kämpf et al. (2013), who report variations from 15 to 50 % from the mean for concentrations of less than 20 %, whereas the deviation was at about 5 % for higher CO₂ soil concentrations.

The rate of discharge at surface was measured using the closed-chamber method; an easy and fast way of estimating the discharge rate of CO₂ as shown in numerous examples in volcanically (Chiodini and Frondini 2001; Carapezza et al. 2009; Ingaggiato et al. 2012) and non-volcanically active degassing zones (Bergfeld et al. 2001, 2006; Byrdina et al. 2009; Chiodini et al. 2010; Lewicki et al. 2012). For this purpose, a West Systems (Italy) device was used. The device uses a LiCOR 820 infrared gas

Fig. 3 Example of the change in the gas flux in $10^3 \text{ g m}^{-2} \text{ day}^{-1}$ and the CO₂ content in soil gas in % around one dry CO₂ vent in the Hartoušov mofette area (DDS), measured on 29 June 2012. The scheme illustrates that the measured gas flux varies within decimetres and centimetres and depends on the placement of the gas flux chamber

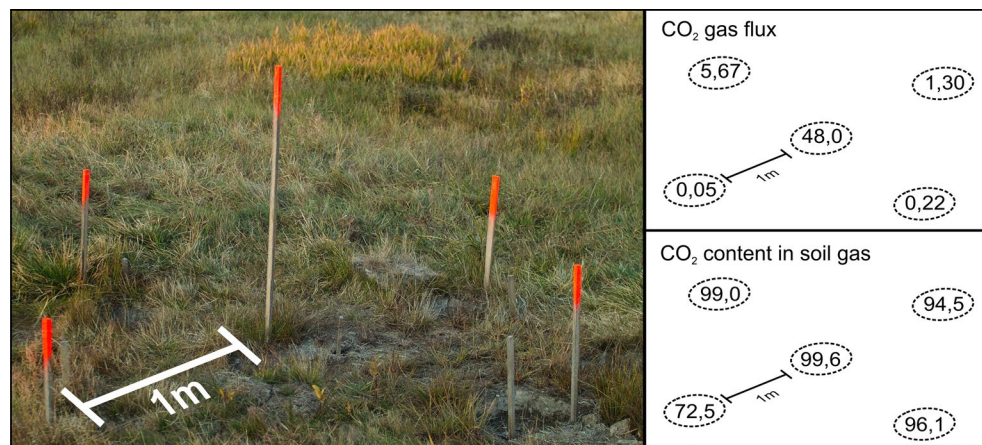
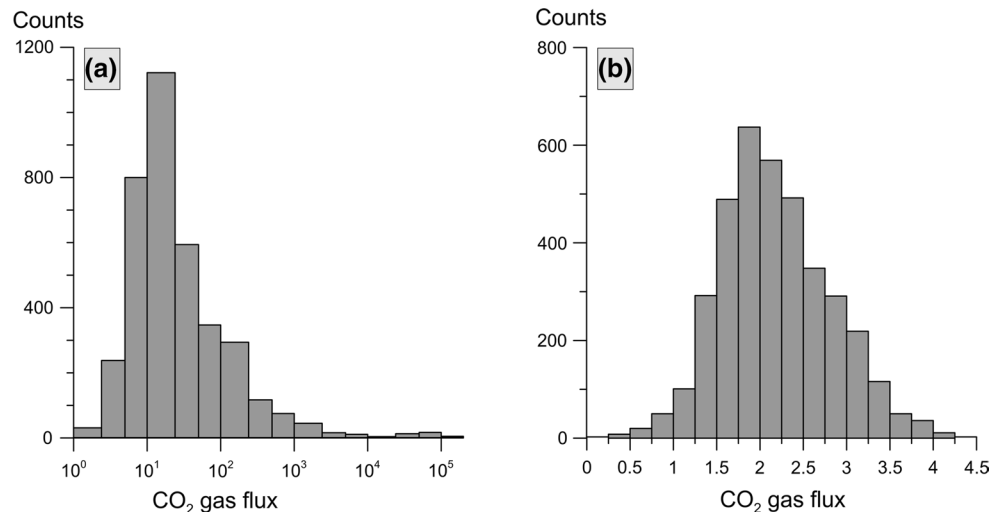


Fig. 4 Histograms of the distribution of 3,770 CO₂ gas flux measurements in the Hartoušov mofette field. **a** Untransformed distribution of the observations with gas fluxes on a logarithmic scale (gas flux in $\text{g m}^{-2} \text{ day}^{-1}$). Even on this logarithmic scale, the distribution is strongly positively skewed. **b** Gas fluxes after the transformation using the Box–Cox transformation with $\lambda = -0.23$

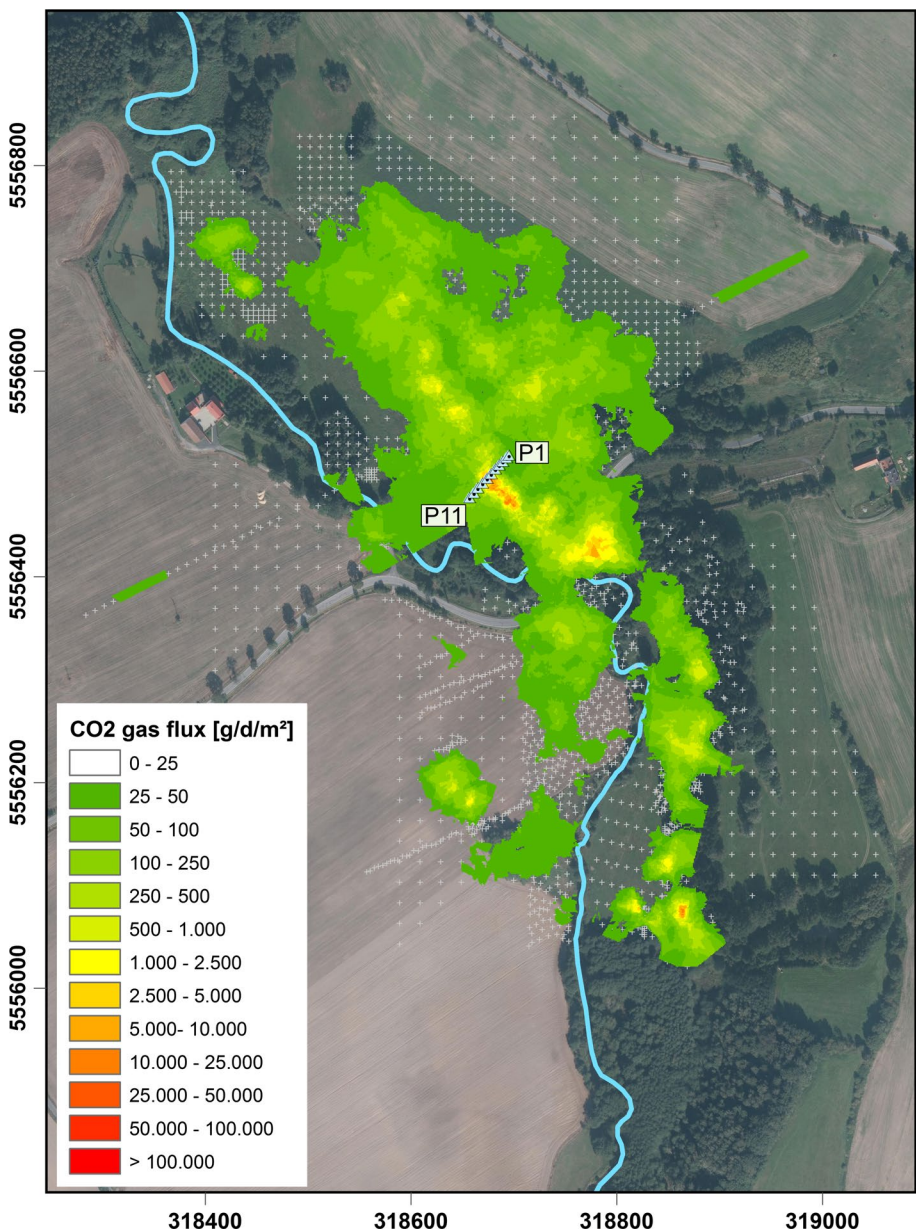


analyser for CO₂ discharge quantification, and the usage of two accumulation chambers ($VA = 2,756 \times 10^{-3} \text{ m}^3$ and $VB = 6,186 \times 10^{-3} \text{ m}^3$) allows for the high-accuracy measurements of gas fluxes up to $600 \text{ mol m}^{-2} \text{ day}^{-1}$ ($\approx 26.5 \times 10^3 \text{ kg m}^{-2} \text{ day}^{-1}$), according to the manufacturer. Within this range, the device has an accuracy of 4 %, higher fluxes increase the uncertainty as the chamber is saturated faster. Air temperature and barometric pressure were recorded and used to calculate the actual gas flux. Fifteen to twenty centimetres of soil coverage was removed several hours before measurement. This way, most of the surface vegetation was removed to establish more equal conditions for the gas flux mapping and to remove most of the influence of biogenic CO₂ input.

Point-to-point spacings varied from $20 \text{ m} \times 20 \text{ m}$ in areas with little CO₂ content soil gas and low fluxes to finer measuring grids ($10 \text{ m} \times 10 \text{ m}$, $5 \text{ m} \times 5 \text{ m}$ and finer spacings below $<1 \text{ m}$) in areas of strong degassing. This procedure accounted for a fast mapping but also aimed at encompassing gas chimneys. Kämpf et al. (2013) claimed that >95 % of the total emitted CO₂ can be attributed to CO₂ vents in the

Hartoušov area, although their diameter is often $<1 \text{ m}$ at the surface (Fig. 3). Detailed measurements around the gas vents were necessary due to the fact that the amount of CO₂ discharged by single vents can be over- or underestimated if the sampling position is shifted only by a few decimetres, which leads to an incorrect evaluation of the CO₂ balance for the area of investigation. This feature was already mentioned in Chiodini et al. (1998), Carapezza and Granieri (2004), who claimed that degassing occurs along microfractures and that consecutive flooding and drying can lead to a different spatial distribution of these microfractures, especially in areas of advanced argillaceous alteration. This is true in our area of interest, the Plesná valley, where clays or clayey sediments dominate as described in drills from GEOFOND (Czech Geological Survey, Fig. 9) and Flechsig et al. (2008). As this vent-bound degassing was exceeding the high-accuracy limitations of our gas flux metre, high gas fluxes bear higher uncertainties: the highest gas fluxes would fill the accumulation chamber within 5 s and the actual flux can only be approximated. In these locations, several measurements were taken to at least partly compensate this effect (Fig. 4).

Fig. 5 Quantified gas flux for 1 m² after interpolation of 3,770 measuring points in the Hartoušov mofette field using trans-Gaussian kriging. White dots indicate the measuring position; small triangles mark the locations of the repeated measurement stations (Table 1). Gas fluxes below 25 g m⁻² day⁻¹ are not displayed. P1 and P11 mark the first and last station of the reference profile for repeated measurements (Table 1)



Repeated measurements were carried out along a NE–SW-striking profile perpendicular to the main degassing area in the HMF in 2012. The profile consisted of 11 stations (P1 to P11) with 5 m distance to each other (Fig. 5). P1 was located at E: 318694; N: 5556518 and P11 was located at E: 318656; N: 5556478. The location of the profile was chosen to encompass low-, medium- and strong-degassing spots. Sandig et al. (2014) used also repeated measurements to evaluate the CO₂ degassing behaviour (analysing the gas composition) at the HMF but used a GPS tool with an accuracy of ±5 m as a reference and, thus, different sample spots each time. The repetition of measurements on fixed locations helps evaluating the consistency of the gas flux over the different field campaigns. Hence,

we established fixed sample stations in our measurements. These measurements were carried out in the morning and late afternoon (Table 1). The gas flux was not measured after rain events to keep the alteration of gas paths within the topmost centimetres as little as possible.

Data analysis

For the quantification of the totally discharged CO₂ in the HMF, we applied different, statistical methods using the geostatistical analysis tools in ArcGis: arithmetic mean, inverse distance weighting, radial basis function, ordinary kriging and trans-Gaussian kriging (utilizing ordinary kriging after data transformation using a power function).

Table 1 Results of repetition measurements of CO₂ gas fluxes during field campaigns along a profile consisting of 11 stations across the main mofette in the HMF in 2012

Date	P1	P2	P3	P4	P5	P6	P7	P8	P9	P10	P11	Sum P1–P11
23/06 PM	15	12	7	72	2,119	27,860	582	12	8	8	49	30,744
24/06 AM	22	14	5	108	2,480	27,562	549	15	11	11	53	30,829
24/06 PM	9	7	6	73	888	19,490	490	8	8	11	61	21,050
25/06 AM	12	7	6	51	1,526	16,792	403	10	8	12	55	18,881
26/06 AM	8	7	5	78	1,659	20,110	412	7	9	12	74	22,380
26/06 PM	5	7	7	67	1,707	29,104	415	9	6	10	60	31,396
27/06 AM	12	9	7	113	2,237	24,268	481	15	10	12	84	27,247
27/06 PM	10	9	5	98	1,683	21,694	437	7	8	11	78	24,039
28/06 AM	18	12	7	129	2,091	32,783	457	14	8	12	73	35,606
29/06 AM	30	13	7	72	1,297	26,542	430	13	12	14	87	28,517
28/08 AM	21	11	8	109	177	13,378	315	42	24	21	258	14,364
29/08 AM	23	7	12	167	1,507	15,335	301	55	30	25	226	17,688
30/08 AM	17	10	3	91	1,733	54,383	334	50	31	20	267	56,939
31/08 AM	10	4	6	64	708	37,298	277	13	17	9	42	38,449
01/09 AM	18	3	3	58	1,007	33,196	255	16	19	7	19	34,602
02/09 AM	18	8	6	103	1,019	17,482	307	23	20	10	23	19,019
08/10 AM	23	3	3	62	388	39,235	26	8	16	3	8	39,774
11/10 AM	19	5	3	33	1,190	46,797	114	7	8	9	9	48,194
Mean	16.1	8.1	5.8	86.0	1,411.9	27,961.6	365.9	17.9	14.2	12.1	84.8	29,984.3
Standard deviation	6.5	3.2	2.1	32.0	635.1	11,152.1	141.9	14.9	7.9	5.2	80.3	11,122.9
Standard deviation (%)	40.1	39.7	36.6	37.3	45.0	39.9	38.8	83.4	55.7	42.9	94.7	37.1

All numbers are gas fluxes in g m⁻² day⁻¹ except for the percentage-based standard deviation. High variations of up to one order of magnitude in the measured gas flux occurred within the course of a day

Arithmetic mean The simplest method for estimations of the total CO₂ discharge in the area is the arithmetic mean. According to Gilbert (1987) and Lewicki et al. (2005), this method can, in the case of a normally distributed population, be used to estimate the amount of ejected CO₂ after calculating the arithmetic mean and standard deviation for 1 m² and multiplying this by the size of area. This method, however, is very susceptible to few very high or low values.

Radial basis function The radial basis function method is an exact interpolator, which means that the interpolated surface has to go through every measured sample value. The method calculates the surface by combining circular hyperboloids, where each hyperboloid is centred on a sampled unit (Lewicki et al. 2005). The continuous surface created this way was then separated into parcels of 1 m², and the specific, calculated gas flux was attributed to each parcel. The closer data points are together, the more weight they have in the interpolation process. Radial basis functions are also applicable to large datasets. However, they are inappropriate when large changes occur within short distance as over- and underestimations will occur in the process.

Kriging Kriging is based on interpolation between sampled points using spatial covariance values. Observations closer to each other are given more weight in the process than observations further away. In this case, we used ordinary kriging, as it is an unbiased estimator that minimises variations in the estimations. Ordinary kriging also often is used in soil science and CO₂ gas studies (Bergfeld et al. 2001; Rogie et al. 2001; Lewicki et al. 2012; De Bortoli Teixeira et al. 2011). Kriging in general underestimates maxima and overestimates minima in the interpolation process (averaging). After the interpolation, the surface was split into 1 m² parcels, and the calculated gas flux was attributed to each parcel.

Trans-Gaussian kriging Most geostatistical approaches are based on the assumption of a Gaussian distribution of the data. This means that the skewness of the dataset should be exactly or close to zero. In our case, this was not the case as it was strongly, positively skewed (see “CO₂ gas flux and CO₂ soil gas concentration” section). Transformation of the dataset before geostatistical analysis and a consecutive back transformation afterwards can be performed to get normally distributed data. A fast way to achieve this is to transform the original data by using a power transform, such as the

Box–Cox transformation [e.g. Box and Cox (1964); Sakia (1992)], where the observed dataset $Z(s)$ is transformed to a normally distributed dataset $Y(s)$ using a suitable parameter λ . The Box–Cox transformation is:

$$Y(s) = \left(Z(s)^{\lambda} - 1 \right) \lambda^{-1} \quad \text{for } \lambda \neq 0$$

A special case is the so-called log-transformation in case when $\lambda = 0$. In our case, using $\lambda = -0.23$ yielded the best results. After the transformation, ordinary kriging was applied to the transformed dataset (see above). This process is also known as trans-Gaussian kriging.

Geophysical investigations: geoelectrical and gravity measurements

Geoelectrical methods are often the first choice for the investigation of near-surface sedimentary structures and processes within these because of their sensitivity to porosity, water and gas saturation of the pore space, salinity and temperature of the pore fluids expressed by the conductivity of the pore fluid and the presence of clay minerals. However, the same factors cause difficulties in the unequivocal interpretation of electrical resistivity images. Complementary information to electrical resistivity measurements is essential to improve their interpretation and is provided in this study by microgravity, CO_2 measurements, and the sedimentological results of drillings [Flechsig et al. 2008, GEOFOND (Czech Geological Survey)]. Modern electrical imaging techniques (or electrical resistivity tomography/ERT) are based on the concept of remapping the same profile with a wide range of electrode spacings and involved both the field measurements by combining sounding and profiling techniques and the algorithms for data inversion. ERT has proven to be reliable for providing realistic images of the spatial distribution of electrical resistivity in the subsurface and has successfully been applied to a wide variety of problems such as environmental survey (Clifford and Binley 2010), characterization of fault zones (Nguyen et al. 2007; Wise et al. 2003; Suski et al. 2010) and geothermal regions (Finizola et al. 2006, 2009, 2010; Revil et al. 2008, 2011). The geoelectrical investigation aimed at detecting characteristic structures, which could be related to CO_2 ascent and the possible evidence of the PPZ in the resistivity distribution.

The aim of microgravity measurement was to determine whether the degassing zones in the Cheb Basin exhibit some mass deficit due to the degassing process. We decided to perform microgravity measurements that could detect zones of mass deficit or decreased rock density related to these phenomena. It may be expected that the gas emission would enlarge the pores in soft near subsurface sediments, as well as contribute to widening of the gas channelling

fractures. Another hypothesis is that uprising fluids are capable of transporting sediments (Flechsig et al. 2008) which leads to a lateral deformation and thus leads to a deformation of the local gravity field. To our knowledge, the application of gravity measurements for research purposes on volcanically non-active, dry degassing sites has not been done before.

Electrical resistivity tomography

The geoelectrical research, which involved the survey of three profiles perpendicular to the assumed course of the PPZ as postulated by Bankwitz et al. (2003b) and the Plesná valley with its diffuse degassing sites of different degassing rates (HMF and BMF), was carried out between April and June 2012 (Fig. 2). They cross the river Plesná valley and the assumed course of the PPZ from W to E with fault scarps of approximately 15–20 m, running roughly parallel to the river. The valley slopes are asymmetric: flat in the west and steeper in the east. Profile No. 1 crosses the PPZ in the vicinity of the Bublák degassing area with several vents of high degassing rates, No. 2 crosses a meadow and fallow land with flatter slopes than on profiles 1 and 3 and lateral expanded degassing zones, and profile No. 3 crosses the valley 500 m south of profile 2, where small, dispersed CO_2 vents were discovered. Using a multi-electrode-device GeoTom (Geolog Fuß and Hepp, Germany), multi-core cables and conventional steel electrodes, the measurement was taken with the Wenner-alpha ($C_1 P_1 P_2 C_2$) and Wenner-beta ($C_1 C_2 P_1 P_2$) configuration, where the electrical potential difference caused by an electrical current, which is injected at electrodes $C_1 C_2$, is measured at $P_1 P_2$. The electrode spacing was 5 m. The used electrode arrays are different in their horizontal and vertical resolution, penetration depth and signal-to-noise ratio. The former has advantage in the signal-to-noise ratio even for measurements with larger offsets, whereas the latter has a higher sensitivity to lateral variations in the resistivity. The lateral position was determined in the field using a Garmin GPS with a precision of ± 3 m.

Different combinations of current and potential pairs of electrodes with increasing separation are measured and result in the combination of sounding and profiling sections with a maximum investigation depth of approximately 80–90 m. The stacking routine of the measurement device ensures a high data quality. In general, the measured values had a standard deviation of less 5 %. The resistivity field data (resistance values obtained from potential measurements and injected current and related geometry information depending on electrode spacing) were inverted in a 2D subsurface model of resistivity distribution. The inversion code DC2DInvRes [Th. Günther, www.resistivity.net and Günther et al. (2006)] which uses a nonlinear

smoothness-constrained least-squares technique to calculate the resistivity of the model blocks and a fast finite-difference operator to generate apparent resistivity values was used to determine a model that adjusted the measured data optimally. An optimization process tries to reduce iteratively the difference between the calculated and measured apparent resistivity values. The per cent error, considering N points of measurements was calculated as a data fit indicator. The final model was obtained using a combined inversion of data from Wenner-alpha and Wenner-beta configurations.

Gravity

A LaCoste and Romberg D-188 gravimeter was used for the gravity surveys after marking each station with wooden pegs. The standard error was about 0.011 mGal in swampy areas (e.g. BMF), while on hard field and hard meadow surface, the error was only 0.004 mGal. The elevation was measured by levelling, while end points were also tied to the national geodetic system by RTK GPS observations, using Trimble hardware. Some points in forest were observed by total station. The spacing between each measurement station was 5 m in the central zones and higher (10–40 m) at the ends of each profile. The accuracy of all these measurements was better than 3 cm in vertical component. Terrain corrections were calculated from an accurate DTM (1 m resolution) to the distance of 2.5 km, and the outer part of the correction to 167 km from SRTM90 DTM. Anyway, there were almost no steep slopes in the area, so that terrain effects were properly compensated, except for the nearest surrounding of the river bed. Because the Plesná valley is part of the Cheb Basin, the reduction density of $2,300 \text{ kg m}^{-3}$ was applied in the formula for the Bouguer gravity anomaly. The regional trend was removed from the data. Different filtering techniques were applied to separate small-scale from large-scale signals. A high-pass filter with 40 m wavelength (“HP40”) was chosen to visualise the effect of the degassing zone. Additionally, a filter with 100 m wavelength and smoothing by trends of the 9th order (“Hp100-Pol9”) was chosen to visualise the change in the overall subsurface geology.

Results

CO_2 gas flux and CO_2 soil gas concentration

Figures 5 and 6 show linear distributions of CO_2 gas efflux and concentrations. In the southern part of the area, the degassing regime is N–S oriented, while in the northern part, the orientation changes to NNE–SSW-oriented degassing. The N–S-oriented degassing occurs in a spatially

narrow area and is lower than in the NW–SE-oriented degassing part, where the emission is stronger and also occurs over a larger area. Furthermore, strong degassing occurs near the bridge/road which crosses the Hartoušov mofette field. Although this could be a naturally occurring phenomenon, it is most likely linked to a disturbance of the natural degassing regime due to the construction works.

The distribution of the measured gas fluxes can be seen in Fig. 4. Measured gas fluxes varied from $<10 \text{ g m}^{-2} \text{ day}^{-1}$ at the margin of the mofette field up to $125,000 \text{ g m}^{-2} \text{ day}^{-1}$ in the centre of CO_2 vents. Most of the measured gas fluxes in the HMF were in the range of $1\text{--}100 \text{ g m}^{-2} \text{ day}^{-1}$. Of the 3,770 measurements in the database, about 96 % of the totally discharged CO_2 could be related to 10 % of the measurements (377 values, $2.53 \times 10^6 \text{ g day}^{-1}$) and 84 % of the total CO_2 could be related to only 37 spots, which is $\approx 1\%$ of all measurements. On the other hand, 3,172 of the 3,770 measurements ($\approx 84\%$) could be related to gas fluxes $<100 \text{ g m}^{-2} \text{ day}^{-1}$ revealing the non-Gaussian distribution of the measured gas fluxes with a highly positive skewness.

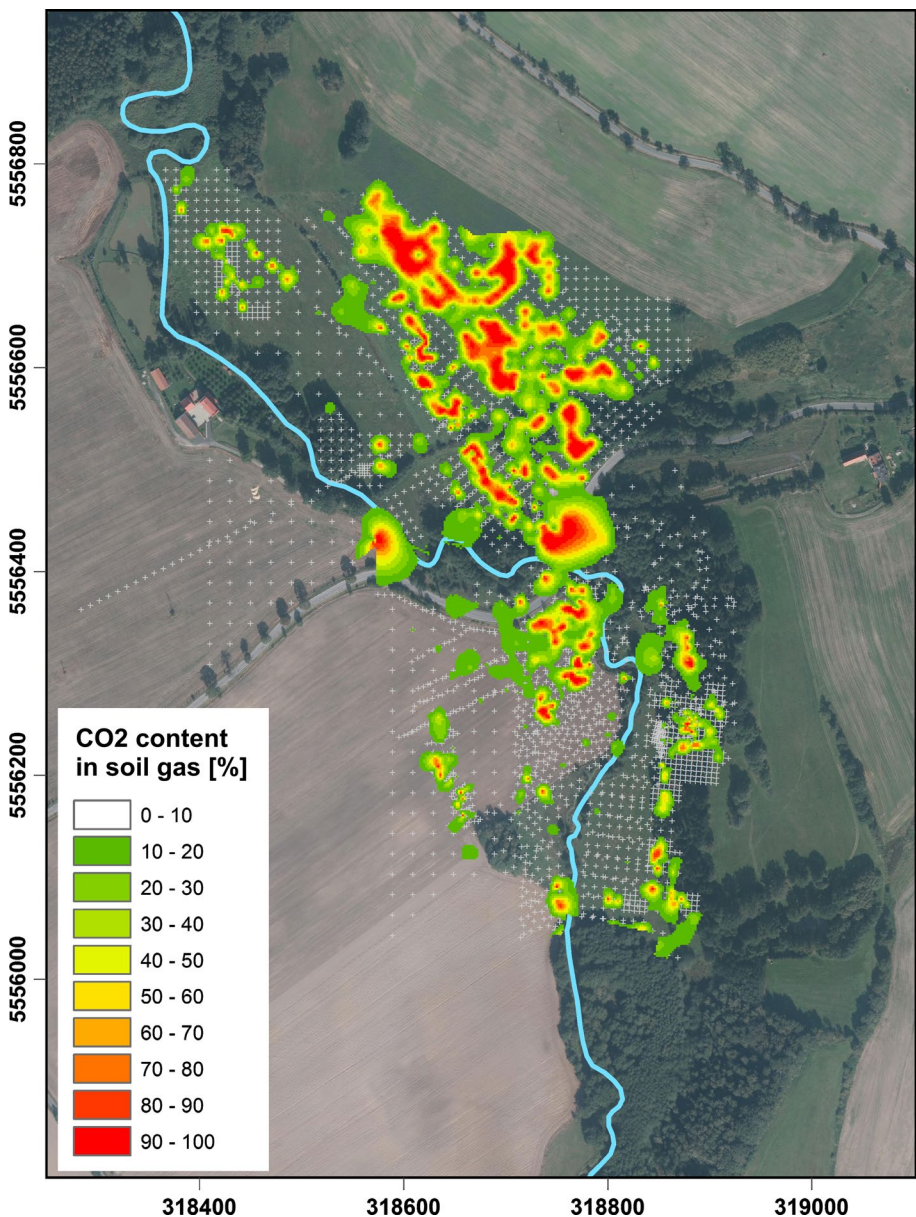
Table 1 shows the results from the repetition measurements in 2012. Variations in the measured gas fluxes could be observed within the course of a day: gas fluxes measured after several hours can differ significantly from another and be higher/lower by up to one order of magnitude for several spots. On average, standard deviations of nearly 40 % from the mean value were noticed along the profile. Considering these large variations is crucial when trying to quantify the amount of daily discharged CO_2 . In most gas flux studies, standard deviations and variations are not shown or they are presented but not discussed in detail. Particularly, at heavily degassing sites, one-time measurements might lead to serious misinterpretations of this site’s CO_2 discharge. The high deviations in the gas flux occur in high- and low-degassing areas.

Calculations of the gas flux within the HMF lead to varying results due to the heavily positively skewed data. All methods have in common that they insufficiently reproduce the impact of the spatially narrow vents within the wide, less-degassing surroundings in the HMF. The non-Gaussian distribution of the degassing leads to very high standard deviations in all methods. The total sums are calculated for each cell of 1 m^2 in the area (347,872 cells).

Arithmetic mean The calculated arithmetic mean and standard deviation for all gas flux measurements results in an average CO_2 gas flux of $697.0 \text{ g m}^{-2} \text{ day}^{-1}$ and a standard deviation of $6,576 \text{ g m}^{-2} \text{ day}^{-1}$. This leads to a calculation of the whole area of $242 \times 10^6 \text{ g m}^{-2} \text{ day}^{-1}$.

Radial basis function Calculations based on the radial basis function result in an average value of $279.9 \text{ g m}^{-2} \text{ day}^{-1}$ with a standard deviation of $1,510 \text{ g m}^{-2} \text{ day}^{-1}$. The overall estimation of the gas flux in the area of the HMF was $97.4 \times 10^6 \text{ g m}^{-2} \text{ day}^{-1}$.

Fig. 6 Distribution of CO₂ content in soil gas in 0.6–0.8 m depth in the Hartoušov mofette field after interpolation of 3,003 measurements. White dots indicate the measuring position. CO₂ contents below 10 % are displayed as hollow

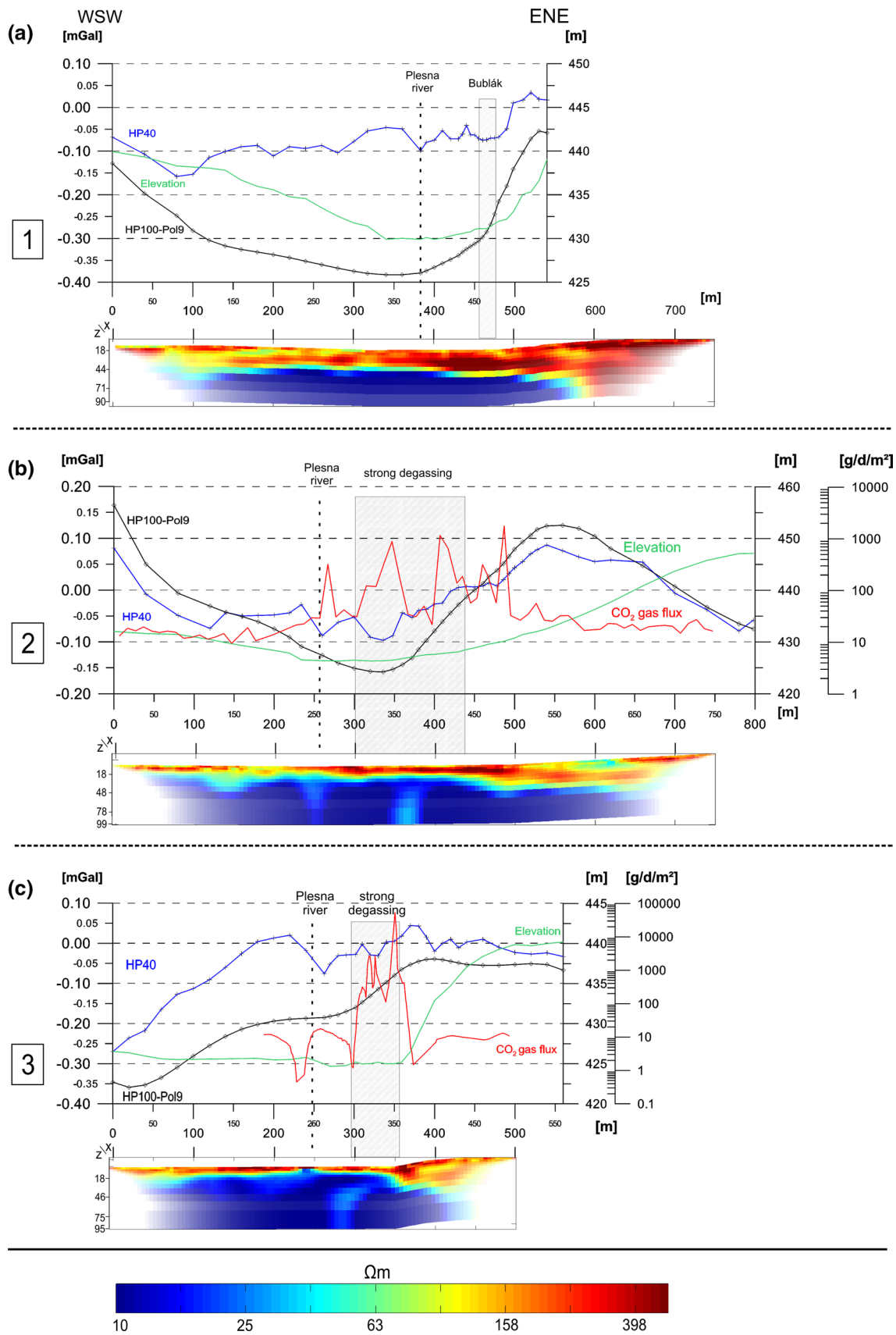


Kriging Geostatistical estimations of the CO₂ gas flux using ordinary kriging results in an average value of 250.7 g m⁻² day⁻¹ and a standard deviation of 2,400 g m⁻² day⁻¹. This method estimated 87.2 × 10⁶ g m⁻² day⁻¹ as the area's daily gas discharge rate.

Trans-Gaussian kriging The lowest standard deviations were achieved after transformation of the dataset and consecutive ordinary kriging. This procedure resulted in an average value of 65.2 g m⁻² day⁻¹ and a standard deviation of 480 g m⁻² day⁻¹. 22.7 × 10⁶ g m⁻² day⁻¹ were calculated as the daily CO₂ gas flux rate for the HMF.

In Fig. 6, results from the CO₂ content at depths of 0.6–0.8 m reveal that the soil contains high amounts of CO₂ over large areas, which replaces free oxygen in areas with

high CO₂ fluxes. Across the mofette field, some areas feature almost complete absence of O₂ at depths below 0.5 m. Saßmannshausen (2010) and Rennert et al. (2011) already showed that in general the CO₂/O₂ ratio decreases towards shallower depths, which is probably linked to atmospheric influence. Annunziatellis et al. (2008, Fig. 7) present a comparison of their CO₂ flux and concentration measurements. In general, high concentrations are found where high gas fluxes are measured, implying that CO₂ vents supply their surrounding with CO₂ and replace O₂ in pores. However, they do not present a direct proportionality between flux and concentration and also cut out fluxes higher than 500 g m⁻² day⁻¹. In the HMF, direct correlations between gas flux and CO₂ content in soil are impossible: while gas flux measurements take place at depths of 15–20 cm after



◀Fig. 7 Results of the ERT and relative gravity along the profiles 1–3 in Fig. 2 after filtering. The tomographies are inverted by using Wenner-alpha and Wenner-beta simultaneously. “HP40” is the gravity after applying a 40-m-wavelength filter on the measured Bouguer gravity. “HP100-Pol9” is the gravity after the application of a 100-m-wavelength filter and a polynomial trend of 9th order. Profiles 2 and 3 also show CO₂ gas flux for comparison. Distinct local gravity lows correspond to high CO₂ flux and increased electric resistivity

removal of the topmost organic layer and require the soil to be dried out, the CO₂ content is measured at depths of 0.6–0.8 m. Within these few decimetres, the CO₂ content and gas flux change significantly (Rennert et al. 2011). The argillaceous composition of the soil and the high, but varying ground water level in the HMF lead to highly variable properties of the soil. High ground water levels lead to water saturation of pores and thus a channel-like degassing, while the first decimetres of soil are usually drier. This leads to open pore space and microfractures which promote rather diffuse degassing. Direct comparisons of CO₂ gas flux and concentration can only be accomplished if the gas flux measurements take place before the soil gas measurement drilling penetrates the exact same position and creates artificial migration paths for ascending CO₂.

Geophysical investigations: geoelectrical and gravity measurements

Geoelectrics

ERT experiments resulted in three profiles, shown in Fig. 2. The inversion results can be seen in Fig. 7a–c. The inversion of the ERT data along the profiles resulted in models with resistivity values between 5 and 1,000 Ohm, the latter appear locally in the near subsurface. To ensure a uniform representation, the resistivity distributions are shown between 10 and 500 Ohm. Generally, on profiles 2 and 3 (Fig. 7b, c), low resistivities of <50 Ohm were measured in the Plesná river valley at depths greater than 5–20 m. These low resistivity are related to clayey sands, clays and mudstones, according to Flechsig et al. (2008) and stratigraphic descriptions of drill cores from GEOFOND drills (drill SA-30/ID 103141, depth: 93 m, E: 3188716, N: 5556349 and drill 1H-31B/ID, depth: 30 m, E: 318713 N: 5556543). This unit is covered by a layer of higher resistivity (>150 Ohm) of 10–20 m, which can be related to sand, gravel and fluvial sediments in general. The eastern flanks of the valley (morphological steps of the PPZ) are also characterised by increased resistivities (>150 Ohm) and a significant thickening of this high-resistivity layer to more than 40 m. This layer's resistivity is notably higher in areas where the strongest degassing occurs at surface. The resistivity distribution along profile No. 1 (Bublák degassing area, Fig. 7a) is slightly different compared to profiles 2 and 3.

An increase of the thickness of the topmost high-resistivity layer from 30 to 40 m and a local increase in the resistivity from about 200 to 400 Ohm around the Bublák mofette (profile 1 at 430–480 m) can be observed. In areas of strong surface CO₂ degassing, anomalies in the otherwise higher conductive clayey unit can be measured at a depth of 30–50 m (profiles No. 2 and 3 in Fig. 7). These anomalies are characterised by a resistivity increase to 80–100 Ohm and are stretched slightly in vertical direction. Some resistivity features occur systematically on profiles. A layer of high resistivity (>150 Ohm) with increasing thickness of 10–20 to 30–40 m to the north is measured at surface. The thickness increases east of the scarp (step-like in the eastern parts of profiles). Below this layer, a spatially limited area of increased resistivity translates to a highly conductive, clayey unit.

Gravity

Figure 7 shows changes in gravity along the profiles 1–3 from Fig. 2. The HP100-Pol9 curve shows the general trend of the gravity from west to east (100 m wavelength filter), while HP40 shows more local gravity residuals after a 40-m-wavelength filter.

In the western parts, we assume a significantly different lithological block (Plesná river sediment depositions). This can be observed in all three profiles in the gravity curve HP100-Pol9. The profiles 2 and 3 show the gas fluxes along these profiles for comparison; gas measurements along profile 1 were impossible (swamp area). In all three profiles, the Plesná river has a small gravitational impact on the nearby stations. A cut-off of the Plesná river across profile 2 (Fig. 7b) at 340 m also effects the nearby stations.

The gravity survey along profile 1 reveals that a 50 negative anomaly of about –0.03 to –0.06 mGal can be identified around the Bublák mofette. This anomaly is significant, especially when considering the gravity effect of the nearby steep slope in the east. The Bublák mofette features concentrated degassing, is about 5 m in diameter and is filled with a water column with a height between 0.7 and 2 m. However, the gravity anomaly is much wider (440–470 m) and hints at a deeper source. This indicates that the gravity low is rather caused by an increase in fractures, pore size and/or pore infilling with gas rather than the pure water infilling of the Bublák mofette.

Gravity observations along profile 2 reveal good correlations between lower gravity and increased CO₂ release, especially at the section between 300 and 440 m where a very distinct local gravity minimum of about –0.06 mGal corresponds to high CO₂ gas flux. At the same place, we see also the minimum of the “longer wavelength” gravity residuals (HP100-Pol9). Neither of these two different gravity residual lows is located around the river at 260 m

(profile 2), where they could be expected due to assumed maximum thickness of alluvial sediments. Since degassing occurs over a wide area and not focused in single spots, it is likely that a wide area is affected by the CO₂. This was also observed in the ERT measurements (Fig. 7, profile 2).

Along profile 3, a more chaotic gravity signal can be observed between the river at 260 m and the steep slope at ca. 360 m. A small but distinct gravity low of about –0.03 to –0.04 mGal can be observed at 330–340 m (HP40) where strong (up to $3 \times 10^4 \text{ g m}^{-2} \text{ day}^{-1}$) surface degassing occurs. This gravity low is located where surface degassing via seeps occurs and above the zone of increased electric resistivity. Similar effects can be observed in other areas where degassing occurs.

In general, both methods detect anomalies in their respective potential where strong surface degassing is measured. The resistivity is increased in the subsurface, whereas the gravity is lower compared to the surrounding. Whether this effect is related to an increase in pore volume or microchannels (Bankwitz et al. 2003b; Kämpf and Bankwitz 2005) and/or subsequent infilling by gas or an upward oriented sediment transport as described by Bankwitz et al. (2003b), Flechsig et al. (2008), is debatable. Gravity and geoelectrics both also detect a shift of the lithological blocks in the eastern part of the Plesná valley where a morphological step emerges. This eastern block is characterised by an increase in the electrical resistivity as well as in its density. The geoelectrical inversion also hints at an increase of the topmost layer towards the north.

Discussion

Methodical aspects

Although the gas fluxes in the Hartoušov area are low in most areas, small depressions within the area can accumulate significant and lethal amounts of carbon dioxide. Strongly degassing areas are often accompanied by a change in the vegetation, e.g. timothy grass (*Phleum pratense*) (Saßmannshausen 2010; Pfanz et al. 2007). In a previous study, Kämpf et al. (2013) tried to quantify the gas flux in the HMF. Kämpf et al. (2013, Tab.2) list $\approx 19,000 \text{ l h}^{-1}$ ($\approx 893,760 \text{ g day}^{-1}$ at standard conditions) as the daily amount of released CO₂ for the Bublák mofette (B2), unequally distributed over seven spots. Compared to our dataset, this means that some of the dry degassing spots in the Hartoušov area release amounts of CO₂ that are comparable to the Bublák mofette and that the amount of carbon dioxide release has previously been underestimated severely. Kämpf et al. (2013) also concluded that the daily CO₂ discharge rate is about $1.56 \times 10^6 \text{ g m}^{-2} \text{ day}^{-1}$ for the measured area and that more than 95 % of the CO₂ is

released via gas vents. However, this approach does not account for the spatial distribution of the measurements. This method is very susceptible to positioning and, thus, just a spot check. Small measurement spacing in heavily degassing areas and wide spacings in less-degassing areas lead to an overestimation of the impact of CO₂ discharge in the HMF's CO₂ balance. Using their measurements and ours combined, we tried to get better insight into the tempo-spatial CO₂ degassing behaviour in the HMF using different geostatistical tools.

In general, all applied geostatistical methods used here are heavily influenced by the high skewness of the measured data. Heavily skewed (non-Gaussian distributed) datasets lead to standard deviations that are much higher than the mean. For this reason, estimations using the simple arithmetic mean resulted in the highest mean and standard deviation and are hence not suited for interpretations. The radial basis function method overestimates the highs and underestimates lows as it tries to fit the interpolation surface through all data points. Therefore, the calculated $97.4 \times 10^6 \text{ g m}^{-2} \text{ day}^{-1}$ can be considered as an overestimation. The CO₂ calculated gas flux of $87.2 \times 10^6 \text{ g m}^{-2} \text{ day}^{-1}$ using ordinary kriging is a little lower but kriging itself weights correlation between points based on the semivariogram which is built by looking at the spatial distribution of the data. This way, the degassing vents are too wide and have too much impact on the CO₂ balance. Due to the method, the surface is smoothed out to result in an overall low error and therefore does not represent anomalies properly (highly degassing vents in a rather low-degassing surrounding). The pre-interpolation transformation using the Box–Cox transformation resulted in the lowest standard deviation of all the methods. According to Saito and Goovaerts (2000), kriging results are better, when the data is normally distributed. $22.7 \times 10^6 \text{ g m}^{-2} \text{ day}^{-1}$ is also the lowest estimation from all methods for the area's gas flux, but underestimates the impact of the degassing vents in the smoothing of the interpolation process.

The real, dry CO₂ discharge rate is supposed to be between 23 and ≈ 97 tons per day for an area of $\approx 350,000 \text{ m}^2$ in the HMF. The high uncertainty might be attributed:

1. The CO₂ gas flux mapping was spread over different years and different times of each year. The gas flux is highly variable on different time scales (Table 1). The variations between datasets of multiple surveys in this area from different times can also be seen in Sandig et al. (2014).
2. The measured CO₂ gas flux is highly dependent on the proper placement of the accumulation chamber. Particularly, around gas vents detailed measurements have to be done to not underestimate the impact of

CO_2 vents by mistake or to miss them at all. Moving the accumulation chambers can lead to underestimations of 1 or 2 orders of magnitude for the CO_2 gas flux (Fig. 3).

3. The measuring device uses a LiCOR 820 infrared gas analyser for CO_2 discharge quantification. Although widely used in gas flux studies, it bears high uncertainties when measuring gas fluxes of several tens of kilograms per day and square metre.
4. Geostatistical tools all have different approaches in the interpolation process, and depending on the method, the estimated CO_2 discharge in the HMF varies.

All these factors combined lead to relatively high uncertainties and errors in the quantification of the CO_2 gas flux in the HMF. Changing the measurement system can decrease these errors; however, the effect of temporal and spatial changes in the CO_2 would require many monitoring stations at surface. More advanced geostatistical approaches, such as the sequential Gaussian simulation (Cardellini et al. 2003; Lewicki et al. 2005; De Bortoli Teixeira et al. 2011), might improve the estimation by a bit.

However, these articles also report that this approach only results in slight improvements of estimation of the CO_2 emission rate. These slight improvements would be significantly lower than the natural variations of the CO_2 gas flux in the field. Therefore, a better approximation of the natural degassing behaviour is only achievable by multiple, continuously measuring monitoring stations.

CO_2 degassing at the HMF

Geoelectrical and gravity measurements reveal small magnitude, but distinct anomalies in the respective potential field where surface degassing occurs. In this case, the subsurface features slightly higher resistivities than the surroundings (e.g. profile 3 at 300 m at a depth of 20–30 m) and measurements of the gravitational field reveal small, negative Bouguer anomalies close to focused CO_2 degassing sites. One possible explanation can be an increase of the size of micropores, as described in Bankwitz et al. (2003a) and Kämpf and Bankwitz (2005). The alteration process of rocks by the long-term influence of the high-pressure CO_2 -water mixture mobilises or dissolves slowly, but continuously, the matrix with the consequence that the microcracks and pores will be relatively larger compared to the surrounding. The CO_2 ascent carries ground water along, and the bubbling CO_2 -water mixture is then capable of transporting sediments with it. An increase in pore volume leads to a decrease in the bulk density, and if these pores are filled with uprising CO_2 , it also leads to a decrease in the conductivity (=increase in the resistivity). Annunziatellis et al. (2008) mention that CO_2 migrates

not only vertically, but also horizontally in soil gas via advective forces and density-driven flows. This might lead to the horizontal change in the saturation of pore fluids and the relation of grain size to gas–water-filled (or-non-filled; Bankwitz et al. (2003b)) pore space, which leads to decreased densities and increased resistivities (Revil and Florsch 2010). Another hypothesis includes a fluid-driven material transport from lower stratigraphic units upwards. Such transport of sediments due to high pressure was described by Bankwitz et al. (2003b), Kämpf et al. (2005) and Flechsig et al. (2008). This can also lead to the formation of larger caverns, as observed by Kämpf and Bankwitz (2005) in the Pliocene Vildštejn formation in the open-cast mine of Nová Ves II (E: 314500, N: 5561540, about 4.5 km NW from HMF) at depths of about 50 m. These caverns can have diameters of several decimetres and be partly filled with sediments (e.g. sand) from lower stratigraphic units which are mobilised and transported by a gas–water mixture. Crystallised gypsum was found at the rim of the cavern which indicates that the caverns were filled with fluids before (Störr, pers. comm., 2002). It is unknown to this point how large these cavities can get, but these caverns were about 1 m in diameter and about 10 m long (Fig. 8). Several of these caverns were found in clusters in the open-cast mine along a 300 m active CO_2 degassing long fault (Bankwitz et al. 2003a). Because no strong gas exhalations (only gas in mineral water) were found directly above the hypocentre in the vicinity of Nový Kostel (Kämpf et al. 2013, Fig. 4), it is assumed that low-permeable rock units (permeability barriers built up by low-permeable rock sequences and sealing processes in and above the seismogenic zone) are capping the active hydraulic system.

The following model was published by Bräuer et al. (2003): permeability barriers keep the permanent mantle fluid flux from further rising. Therefore, fluid overpressure is very likely to build up in the surroundings of the hypocentres and stimulate the nearly permanent seismic activity of the Nový Kostel focal zone. The model of Bräuer et al. (2003) is also supported by seismological investigations of Alexandrakis et al. (2014), who found structures in the hypocentral area acting as a fluid trap zone.

ERT measurements reveal an increase of thickness of the topmost high-resistivity layer from south to north. The thickness is about 10 m in the southern and central area of Hartoušov, 15–20 m in the northern area and about 40 m in the Bublák area (Fig. 7). This is most likely related to the Pleistocene sediments of the Plesná valley. Flechsig et al. (2008) found this correlation between these sedimentary layers and an increase in electric resistivity in the main degassing area.

According to the results of pedological and sedimentological investigations at the central part of the HMF (Flechsig et al. 2008; Rennert et al. 2011), we assume the vents to

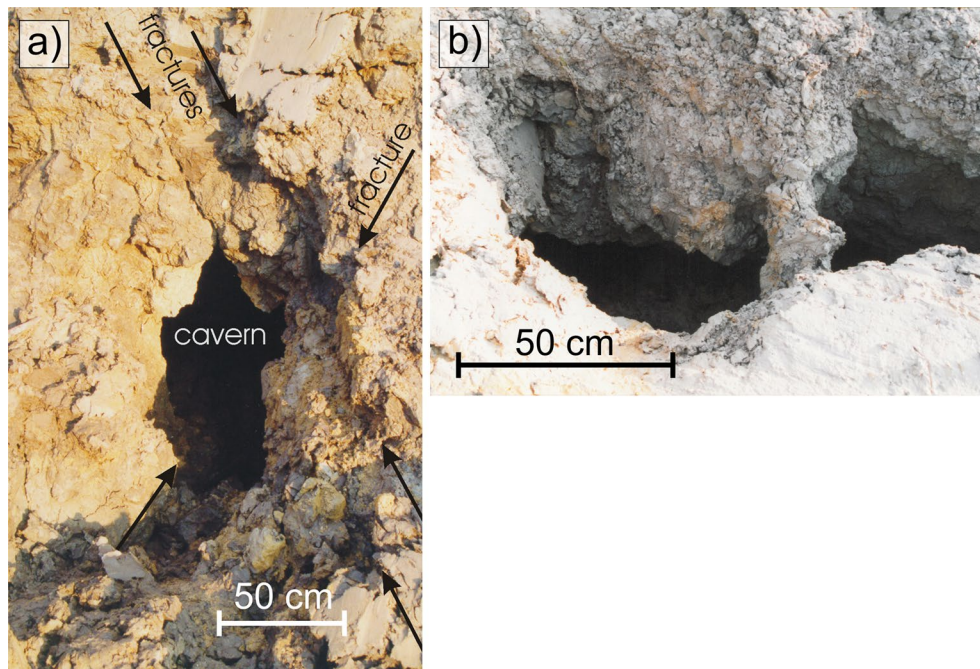


Fig. 8 A cavern in kaolinite-bearing clay in the Vildštejn formation (Pliocene) in the open-cast mine Nová Ves II at 50 m depth, which developed at the intersection of two fracture sets. Mobilised sand

from lower stratigraphic units filled the cavern at the base and was found nearby. Gypsum crystals are found at the rim of these caverns. **a** Front view, modified after Kämpf and Bankwitz (2005). **b** Top view

be more or less stable in the basement and the sedimentary subsurface along fractures. However, the first few metres of soil (Quaternary gravel and sand with varying contents of clay) seem to be responsible for a lateral change of the gas seepage. Weather effects, such as rain or soil frost, seem to change the pathways for the uprising CO₂ (Chiodini et al. 1998; Carapezza and Granieri 2004). This can be observed visually, when the position of the wilted vegetation changes (Pfanz et al. 2007) within seasons and over the years, and technically via gas flux measurements (Table 1). Similar observations were made in the HMF by Sandig et al. (2014). They report different levels of CO₂ in the soil, depending on atmospheric conditions and soil properties. On the other hand, their measuring positions changed with every survey, which is a major source of errors as the CO₂ presence changes on a submeter scale. They find weak anomalies in soil temperature and soil moisture at the degassing spots, but also find these where no CO₂ degassing occurs. Hence, quantifications of the totally released CO₂ via the closed-chamber method can only be approximated. As large amounts of CO₂ are released via gas vents with diameters <1 m, changes in time and position of the measurement can result in high uncertainty of the CO₂ gas flux estimation. Girault et al. (2014) listed total amounts of CO₂ discharges for volcanic, geothermal, hydrothermal, mofette and fault-related areas. The HMF is also present in this list, referring to the statements from Kämpf et al.

(2013). As this study provides new information about the degassing process at this site and Kämpf et al. (2013) only made a minimum estimation of the gas flux, we suggest using the values provided in this article for the HMF for future comparisons.

The Počátky-Plesná fault zone

The regional fault network along the N–S-striking Regensburg–Leipzig–Rostock zone is characterised from the area of Regensburg to Leipzig by high number of N–S-, NW–SE- and sometimes also E–W-striking local faults (Bankwitz et al. 2003b). According to Bankwitz et al. (2003b), the Mariánské Lazně fault (MLF) consists south-east of Nový Kostel of four parallel trending faults which have been active recently. Both the Mariánské Lazně fault system and the Počátky-Plesná zone feature combinations of N–S- and NW–SW-oriented sub-faults. The boundaries of the pull-apart basin-like structures fit exactly this combination of fault orientations.

Bankwitz et al. (2003b, Fig. 6b) investigated the course of the PPZ from the NKFZ southward for about 6–7 km to U Mostku. Our investigations continued the research of the PPZ in the HMF. We agree with the results of Havíř (2000), Bankwitz et al. (2003b), Peterek et al. (2011) and Kämpf et al. (2013), as we can continue the split course of the PPZ in southward direction. We agree with the suggestion of

Bankwitz et al. (2003b) that the PPZ composed of differently running segments can be continued morphologically southward: NNE-running (015° strike) and NNW-running (150° – 160° strike) segments. Degassing occurs along the eastern margin of the PPZ, which retraces at least one NNE- and one NNW-running segment. Kämpf et al. (2013) also present other degassing-related phenomena like ochre springs (as a sign for mineral water) along the PPZ north of the HMF and BMF which support the hypotheses of Bankwitz et al. (2003b) and its course along two differently striking segments. Our measurements show two types of CO_2 degassing behaviour related to these two differently striking areas: degassing along the N–S segments is spatially narrow and less intense compared to the NW–SE-striking segment, where degassing is stronger and affects a wider area. It is to be noted that the wet mofettes of the BMF are also located along NW–SE-striking segments of the PPZ.

As postulated by Bankwitz et al. (2003b) and supported by Peterek et al. (2011) and Rojík et al. (2010), we also agree that the eastern block along the fault has experienced some kind of tectonic movement. Bankwitz et al. (2003b) postulate a “true level difference” between eastern and western flank of 5–15 m, whereas Peterek et al. (2011) postulate 12 m of difference. However, Bankwitz et al. (2003b) also mention a difference in elevation of up to 29 m. Unfortunately, Peterek et al. (2011) mistook the postulates from Bankwitz et al. (2003b) as they mixed level difference (vertical displacement of stratigraphic units) and scarp height. Thus, both articles are in agreement in terms of the displacement along the fault scarp.

Figure 9 shows the stratigraphic units of two GEOFOND drills near the Hartoušov village. SA-30 is located within the Plesná valley and HV12 is located on the eastern block. The lateral distance between drill wells is about 250 m. The thickness of the Neogene sediments is significantly increased (79 m in the western part, 107 m in the eastern part). While a 2.7-m-thick coal layer and a 25-m-thick layer of Palaeozoic eluvium were identified in the HV12 drill, these layers were not found in the SA-30 drill. The basement (Palaeozoic mica schists) has an offset of about 40 m between the two drills. This discrepancy between total elevation difference and stratigraphy difference might be related to the fact that the eastern flank experienced subsidence during the formation of the Cheb Basin during the late Oligocene to Mid Miocene (Špicáková et al. 2000; Peterek et al. 2011). Špicáková et al. (2000, Fig. 10) already showed that the thickest deposits of the Late Pliocene Vildštejn formation are not bound to the course of the MLFZ, but is aligned in a rather N–S-trending course. Subsequently, Peterek et al. (2011) show that the eastern flank experienced uplift during and after the Middle Pleistocene. This reactivation along the PPZ leads to the 12 m in geological shift

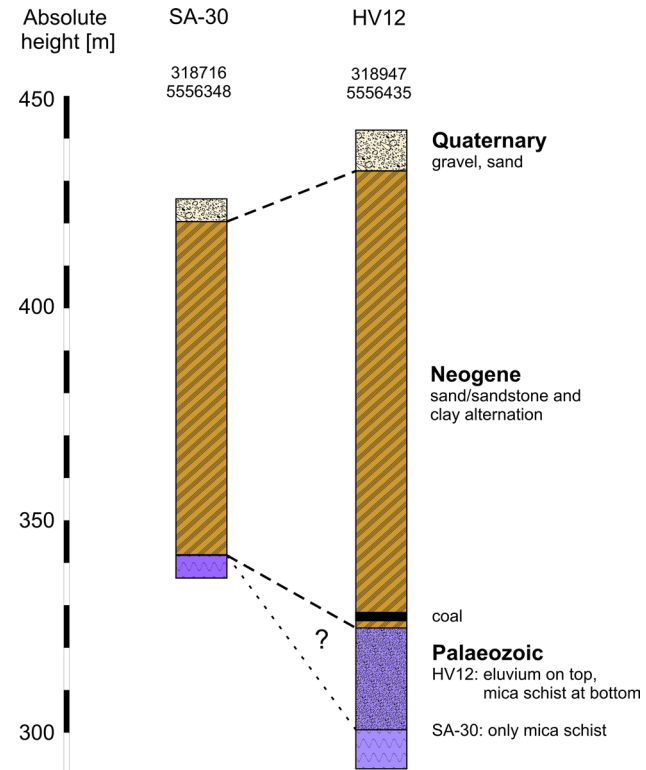


Fig. 9 Stratigraphic profile of the GEOFOND drill cores SA-30 and HV12 and their respective coordinates. The location of the drills can also be seen in Fig. 10

between the top of the Neogene sediments and 20–30 m elevation shift nowadays. Peterek et al. (2011) also mention that the southward continuation of the PPZ (the so-called Nebanice Fault Zone) features change in the displacement rate over time. This was found out after they did research on terraces at the Ohře river and their displacement to each other between the western and eastern blocks.

Sandig et al. (2014) find a change in their self-potential measurements in the eastern part of their profile and interpret this as the fault scarp of the PPZ. Our findings in the local electrical resistivity of profile 1–3 show a thickening of the high-resistivity block in the east in the ERTs, which we interpret as fault scarps (Fig. 7). The increase in the gravity towards the east contributes to this assumption. A GPR (Ground Penetrating Radar) profile crossing the Bublák mofette in E–W direction, and thus very near to the geoelectric profile No. 1, featured in Hubatka et al. (2004) shows a similar result. They find a 200-m-wide and 10-m-deep depression (15 m near the Bublák mofette) on top of a complex fault pattern. Although visible in Hubatka et al. (2004, Fig. 1), the authors do not describe the distinct and sudden shift in the lateral rock composition underneath the morphological step, which is most likely related to the PPZ. They interpret this anomaly as an indicator for

the fault scarp near the surface. All of these articles and our studies fit the drilling results, shown in Fig. 9.

The PPZ's importance on the regional geodynamic activity is, from our point of view, underestimated. Particularly, seismological interpretations of earthquake swarm activity of the last decades linked the earthquake swarm activity with fault planes of the MLFZ, as it is the morphologically most striking one (Grünthal et al. 1990). However, as already mentioned by Bankwitz et al. (2003b), most of these focal mechanisms show a rather N–S sinistral strike-slip movement for several earthquake swarms (1985/1986, 1994, 1997, 2000) (Horálek et al. 2000), with only a minor relation to the course of the MLFZ. Fischer and Horálek (2003), Fischer and Michálek (2008) and Vavryčuk (2011) mentioned the planar character of the Nový Kostel focal zone (169° strike). They also admit that more than 90 % of the events were related to this strike orientation. Less activity could be correlated to the strike of the MLFZ. It is also mentioned that previous earthquake swarms in 1985/1986 (Vavryčuk 1993) and 2000 (Fischer 2003) have focal mechanisms with a similar orientation. The most recent comprehensive work on earthquake swarm in NW Bohemia (Fischer et al. 2014) also mentions that prevailing studies on focal mechanisms in the Nový Kostel area mostly feature strikes that are N–S related (165° – 180°) and reflect the course of the PPZ rather than the MLFZ. Furthermore, from long-term geodetic monitoring, Mrlina and Seidl (2008) defined an active tectonic displacement zone of N–S to NNE–SSW direction, rather than NW–SE of the MLFZ.

According to Malkovský (1987), Špičáková et al. (2000), Bankwitz et al. (2003b) and Peterek et al. (2011), the MLFZ played a major role in the development of the Cheb Basin in the Late Tertiary (Oligocene), but showed little activity until the late Pliocene. In the late Pliocene, activity along the MLFZ increased, and the fault was reactivated (Fischer et al. 2014). At present, the PPZ is the seismically more active zone.

Pull-apart basin-like formations along the PPZ?

Bankwitz et al. (2003b) and Peterek et al. (2011) report the sinistral movement of the PPZ around the HMF. Peterek et al. (2011) observed this movement to the south to the Ohře River, and Wendt and Dietrich (2003) measured mainly NNW–SSE-striking sinistral strike-slip movement to the north. Field observations and measurements reveal that the most intense CO_2 degassing occurs over a wide area in the HMF and at BMF, which are located on the NW–SE-striking fault segments. We measured less intense, laterally narrow degassing in the southern part of the HMF, which is N–S oriented. Most of the wet mofettes (see Kämpf et al. (2013)) are also aligned like pearls on a string in a NNW–SSE orientation parallel to the morphological step, while some of them

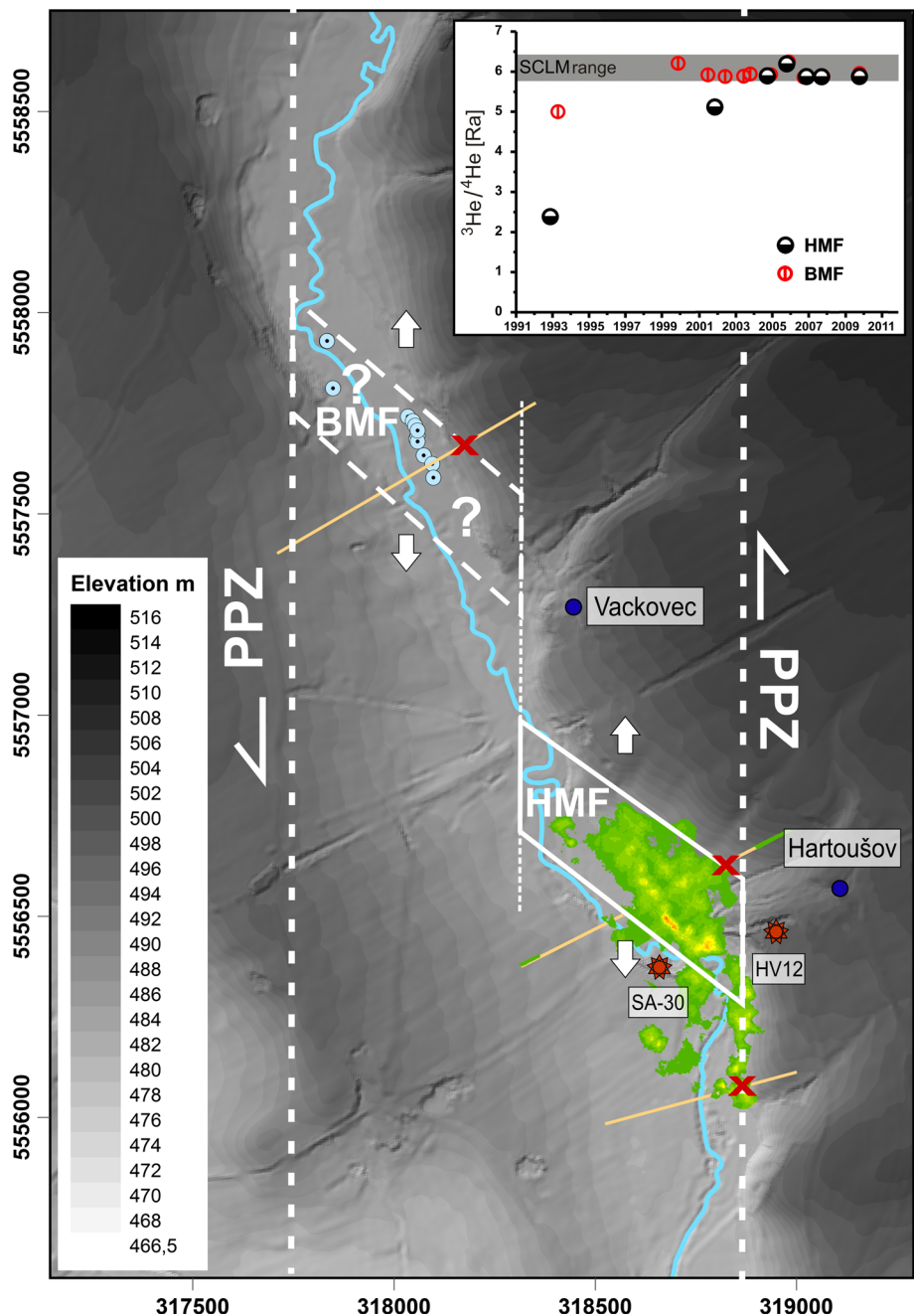
(BNW, B1 and B2) are located further to the north-west and rather isolated. In Bankwitz et al. (2003b) and Peterek et al. (2011), the faults segments were interpreted as sinistral P (=NNE) and sinistral Riedel shears (=NNW). We present a hypothesis that the HMF and BMF represent pull-apart basins, which requires verification in the future.

Pull-apart basins are often the result of two or more blocks moving along strike-slip faults (Aydin and Nur 1982; Brighster et al. 2002; Gürbüz 2010), which was also proven experimentally by e.g. McClay and Dooley (1995) and Atmaoui et al. (2006). The strike-slip movement along the fault leads to compressional or extensional deformation and results in a rhombic-shaped opening with length-to- ratios of mostly 3:1 or 4:1 (Gürbüz 2010). Pull-apart basins can feature sizes of just some tens of metres or several kilometres (Aydin and Nur 1982). This could explain why the N–S-oriented segments (focused and narrow vent degassing in the southern HMF and at BMF) feature a rather steep morphological step, which indicates parallel segments of the fault zone. On the other hand, the central and northern parts of the HMF feature a gentle slope to the west and more diffuse degassing over a wider area, which indicates the extensional basin opening. In this case, it is likely that more of these “basins” exist along the PPZ. One of these structures could be located at U Mostku, as Flechsig et al. (2010) found a basin-like depression via ERT surveys. Aydin and Nur (1982) and Gürbüz (2010) also mention the occurrence of springs and volcanic cones in pull-apart basin areas due to a thinning of the crust. Even though no recent volcanic activity is known in the HMF, it is interesting that the highest ratio of mantle-derived gasses in Central and Western Europe is observed at the BMF and the HMF (Bräuer et al. 2008; Kämpf et al. 2013), indicating easier upward migration paths for fluids.

Gas emanation studies of Weinlich et al. (1999), Bräuer et al. (2003, 2008, 2011) and Kämpf et al. (2013) showed that the CO_2 -dominated gas exhalations exhibit signatures that are related to the subcontinental lithospheric mantle. Bräuer et al. (2011) observed ${}^3\text{He}/{}^4\text{He}$ ratios of approximately 5.89 Ra at Bublák and 5.56 Ra at U Mostku (located along the PPZ), whereas ${}^3\text{He}/{}^4\text{He}$ ratios of approximately 4.60 Ra at Kopanina and 5.13 Ra at Dolní Častkov (located along the MLFZ) were observed, which indicates less mixing of mantle gas with gas from the earth's crust. The highest increase in the ${}^3\text{He}/{}^4\text{He}$ ratios, however, was observed at the Hartoušov mofettes (2.38 Ra in 1993 to 5.11 Ra in 2002 and 5.89 in 2005 (Bräuer et al. 2009)). From 2005 to 2012, the ${}^3\text{He}/{}^4\text{He}$ ratios of gas in the HMF (H5) and BMF (B2) both plot in the SCLM range (Fischer et al. 2014). This might also indicate that BMF and HMF are two separate structures and are on top of separate conduits for CO_2 -dominated gas ascent (Fig. 10, inset).

A possible interpretation is shown in Fig. 10. In this case, the HMF and BMF would represent two small, independent

Fig. 10 Hypothetical model of the HMF and BMF as pull-apart basins (white rhombs) in the sinistral strike-slip-oriented PPZ (white, dashed line). Red stars mark the locations of the drills SA-30 and HV12 (Fig. 9). Red crosses mark the locations where evidence for the segments of the PPZ was found. The results from the gas flux studies (Fig. 5) and the locations of the wet mofettes as well as the geophysical profiles are presented for orientation purposes. Inset change of the ${}^3\text{He}/{}^4\text{He}$ ratio in the gas from the BMF and HMF over time (mofettes B2 and H5, respectively, from Kämpf et al. (2013), inset modified after Fischer et al. (2014)). SCLM subcontinental lithospheric mantle range for ${}^3\text{He}/{}^4\text{He}$ (Gautheron et al. 2005)



basin-like structures which developed at different faults of the PPZ. We interpret this as two independent basins because no gas emanations were observed between the two fields, the thickness of the sedimentary cover in both areas is different and because of the long-lasting trend of the helium isotope ratio only increased slightly in the BMF but significantly in the HMF over the last two decades (Fig. 10, inset). It is likely that similar degassing structures exist further to the north and south of HMF and BMF although they have not been observed yet. Only the occurrence of ochre springs (Kämpf et al. 2013) and the occurrence of mineral springs (Weinlich et al. 1999; Bräuer et al. 2011, 2014; Kämpf et al. 2013)

along the PPZ is well documented as emanations of the magmatic process below. Future studies should focus on systematic search of further degassing centres, and maybe pull-apart basins, following the morphology and regional fault network.

Conclusions

This study presents the results of a multi-method approach on a diffuse degassing structure, the Hartoušov mofette area in the geodynamically most active area of the European Cenozoic Rift System (Bräuer et al. 2008).

1. We discovered that in earlier studies, the degassing behaviour along the Počátky-Plesná fault zone was underestimated by only studying the degassing behaviour of wet mofettes (Weinlich et al. 1998, 1999). As degassing can easily be observed visually in water-filled pools, the detection of dry, and thus optically invisible, CO₂ vents is more problematic, because of their size and temporal and spatial instability.
2. The experiments carried out here show that coarse measuring grids for CO₂ gas flux studies cannot be applied in this diffuse degassing area, as the strongest degassing is related to spots with diameters in the sub-meter scale. Even the best statistical approaches might not correctly quantify the CO₂ discharge in the HMF if not based on thorough and extensive field work.
3. Field experiments show that in this special area, measured gas fluxes at the surface are highly variable, both spatially and temporally. Narrow measurement spacings at CO₂ vents improve the quality CO₂ surveys, and for correct evaluations of the carbon dioxide discharge, monitoring stations are necessary.
4. Due to the non-Gaussian distribution of the measured data, geostatistical tools can only be used to roughly estimate the total CO₂ discharge. Depending on the method, we estimate that between 23 and 97 tons of CO₂ are ejected every day for this area in the HMF via dry seepage.
5. The application of geophysical methods such as ERT and gravity measurements reveals distinct anomalies in the subsurface below strong degassing areas. These anomalous areas are most likely the result of the force behind ascending fluids and consecutive sediment alteration and/or transport linked with the ascent of the CO₂-rich fluids.
6. ERT and gravity surveys also support the theory of a significant shift in the lithological composition between eastern and western flank along the PPZ. The correlation of stratigraphic units between different blocks of the PPZ leads to the assumption that the PPZ has been active since at least the late Miocene and earthquake focal mechanisms indicate that it is still active up to this day. Its importance should be reconsidered, as this fault zone of several tens of kilometres seems to play a major role in the regional tectonic frame.
7. Our results fit into a model in which the HMF and BMF are in the centres of two independent pull-apart basin-like structures, opened by sinistral strike-slip movement along the PPZ.
8. The gas emanations in these pull-apart basin-like structures bear signatures from the subcontinental lithospheric mantle and are thus connected via conduits to it.
9. Future studies should consider the geologic structure and evolution of these two basins related to mantle degassing by seismic profiling, CO₂ gas flux studies and by investigations of drill cores.
10. Since HMF and BMF only illustrate examples along the N–S-striking PPZ, the role of the PPZ and other N–S-striking faults of the RLRZ for upper mantle degassing might have been underestimated previously.
11. More degassing centres might be located along the PPZ south or north of HMF and BMF. Systematic search of further degassing centres, and maybe pull-apart basins, following the morphology and regional fault network might be able to trace more degassing centres.

Acknowledgments We would like to express our gratitude to the German Research Foundation (DFG) for funding this project (KA902/9 and/16 and FL271/13). We thank J. Schumann for his initial hard field work and I. Schüller, S. Kämpf, B. Friedrichs, E. Seidl, M. Seidl and V. Polák for their help in the field during this stage of the project. We want to give warm thanks to N. Wetzig for his language and spelling check. We thank P. Rojik for his help with the interpretation of the drill logs in the Hartoušov area. We also thank the GFZ for financial help for repairing measuring devices. Gravity observations were partly supported by the project CzechGeo/EPOS, Grant No. LM2010008. At last, we like to express our gratitude towards W. H. Geissler, our editor, and Svetlana Byrdina and Domenico Granieri, our reviewers, for their helpful suggestions which improved this article a lot.

References

- Alexandrakis C, Calò M, Bouchaala F, Vavryčuk V (2014) Velocity structure and the role of fluids in the West Bohemia Seismic Zone. *Solid Earth* 5:863–872
- Annuzziatellis A, Beaubien SE, Bigi S, Giotoli G, Coltellà M, Lombardi S (2008) Gas migration along fault systems and through the vadosezone in the Latera caldera (Central Italy): implications for CO₂ geological storage. *Int J Greenh Gas Control* 2:353–372
- Arts RJ, Baradello J, Girard F, Kirby G, Lombardi S, Williamson P, Zaja A (2009) Results of geophysical monitoring over a leaking natural analogue site in Italy. *Energy Proc* 1:2269–2276
- Atmaoui N, Kukowski N, Stöckhert B, König D (2006) Initiation and development of pull-apart basins with Riedel shear mechanism: insight from scaled clay experiments. *Int J Earth Sci* 95:225–238
- Aydin A, Nur A (1982) Evolution of pull-apart basins and their scale independance. *Tectonics* 1(1):91–105
- Babuška V, Plomerová J (2008) Control of paths of Quaternary volcanic products in western Bohemian Massif by rejuvenated Variscan triple junction of ancient microplates. *Stud Geophys Geod* 52:607–629
- Bankwitz P, Bankwitz E, Bräuer K, Kämpf H, Störr M (2003a) Deformation structures in Plio- and Pleistocene sediments (NW Bohemia, Central Europe). In: Van Rensbergen P, Hills R, Maltmann AJ, Morley CK (eds) Subsurface sediments mobilization. Geol. Soc. London, Spec. Publ
- Bankwitz P, Schneider G, Kämpf H, Bankwitz E (2003b) Structural characteristics of epicentral areas in Central Europe: study case Cheb Basin (Czech Republic). *J Geodyn* 35:5–32

- Bergfeld D, Fraser G, Janik CJ (2001) Elevated carbon dioxide flux at the Dixie Valley geothermal field, Nevada; relations between surface phenomena and the geothermal reservoir. *Chem Geol* 177:43–66
- Bergfeld D, Evans WC, Howle JF, Farrar CD (2006) Carbon dioxide emissions from vegetation-kill zones around the resurgent dome of Long Valley caldera, eastern California, USA. *J Volcanol Geotherm Res* 152:140–156
- Box GEP, Cox DR (1964) An analysis of transformations. *J R Stat Soc Ser B* 26:211–252
- Bräuer K, Kämpf H, Strauch G, Weise S (2003) Isotopic evidence ($^3\text{He}/\text{He}$, $\delta^{13}\text{C}_{\text{CO}_2}$) of triggered intraplate seismicity. *J Geophys Res* 108(B2):2070. doi:[10.1029/2002JB002077](https://doi.org/10.1029/2002JB002077)
- Bräuer K, Kämpf H, Niedermann S, Strauch G (2005) Evidence for ascending upper mantle-derived melt beneath the Cheb basin, Central Europe. *Geophys Res Lett* 32:L08303. doi:[10.1029/2004GL022205](https://doi.org/10.1029/2004GL022205)
- Bräuer K, Kämpf H, Niedermann S, Strauch G, Tesař J (2008) The natural laboratory NW Bohemia—comprehensive fluid studies between 1992 and 2005 used to trace geodynamic processes. *Geochem Geophys Geosyst* 9:L17309. doi:[10.1029/2007GL039615](https://doi.org/10.1029/2007GL039615)
- Bräuer K, Kämpf H, Strauch G (2009) Earthquake swarms in non-volcanic regions: what fluids have to say. *Geophys Res Lett* 36:L17309. doi:[10.1029/2009GL039615](https://doi.org/10.1029/2009GL039615)
- Bräuer K, Kämpf H, Koch U, Strauch G (2011) Monthly monitoring of gas and isotope compositions in the free gas phase at degassing locations close to the Nový Kostel focal zone in the western Eger Rift, Czech Republic. *Chem Geol* 290:163–176. doi:[10.1016/j.chemgeo.2011.09.012](https://doi.org/10.1016/j.chemgeo.2011.09.012)
- Bräuer K, Kämpf H, Strauch G (2014) Seismically triggered anomalies in the isotope signatures of mantle-derived gases detected at degassing sites along two neighboring faults in NW Bohemia, central Europe. *J Geophys Res Solid Earth* 119:5613–5632. doi:[10.1002/2014JB011044](https://doi.org/10.1002/2014JB011044)
- Brigster BS, Stephens WC, Norman GA (2002) Structure, stratigraphy, and hydrocarbon system of a Pennsylvanian pull-apart basin in north-central Texas. *AAPG Bull* 86:1–20
- Byrdina S, Revil A, Pant SR, Koirala BP, Shrestha PL, Tiwari DR, Gautam UP, Shrestha K, Sapkota SN, Contraires S, Perrier F (2009) Dipolar self-potential anomaly associated with carbon dioxide and radon flux at Syabru-Bensi hot springs in central Nepal. *J Geophys Res Solid Earth* 114(B10):B10101. doi:[10.1029/2008JB006154](https://doi.org/10.1029/2008JB006154)
- Caine JS, Evans JP, Forster CB (1996) Fault zone architecture and permeability structure. *Geology* 24:1025–1028
- Carapezza ML, Granieri D (2004) CO_2 soil flux at Vulcano (Italy): comparison between active and passive methods. *Appl Geochim* 19:73–88
- Carapezza ML, Ricci T, Ranaldi M, Tarchini L (2009) Active degassing structures of Stromboli and variations in diffuse CO_2 output related to the volcanic activity. *J Volcanol Geotherm Res* 182:231–245
- Cardellini C, Chiodini G, Frondini F (2003) Application of stochastic simulation to CO_2 flux from soil: mapping and quantification of gas release. *J Geophys Res* 108:B9. doi:[10.1029/2002JB002165](https://doi.org/10.1029/2002JB002165)
- Chiodini G, Frondini F (2001) Carbon dioxide degassing from the Albani Hills volcanic region, Central Italy. *Chem Geol* 177:67–83
- Chiodini G, Cioni R, Guidi M, Raco B, Marini L (1998) Soil CO_2 flux measurements in volcanic and geothermal areas. *Appl Geochem* 13:543–552
- Chiodini G, Frondini F, Cardellini C, Granieri D, Marini L, Ventura G (2001) CO_2 degassing and energy release at Solfatara volcano, Campi Flegrei, Italy. *J Geophys Res* 106(B8):16213–16221
- Chiodini G, Granieri D, Avoni R, Caliro S, Costa A, Minopoli C, Vilardo G (2010) Non-volcanic CO_2 Earth degassing: case of Mefite d'Ansanto (southern Apennines), Italy. *Geophys Res Lett*. doi:[10.1029/2010GL042858](https://doi.org/10.1029/2010GL042858)
- Clifford J, Binley A (2010) Geophysical characterisation of riverbed hydrostratigraphy using electrical resistance tomography. *Near Surf Geophys* 8:493–501
- Credner H (1876) Das vogtländisch-erzgebirgische Erdbeben vom 23. November 1875. *Z Ges Naturwiss* 48:246–269
- Dahm T, Fischer T, Hainzl S (2008) Mechanical intrusion models and their implications for the possibility of magma-driven swarms in NW Bohemia region. *Stud Geophys Geod* 52:529–548
- De Bortoli Teixeira D, Panosso AR, Cerri CEP, Pereira GT, La Scala N (2011) Soil CO_2 emission estimated by different interpolation techniques. *Plant Soil* 345:187–194. doi:[10.1007/s11104-011-0770-6](https://doi.org/10.1007/s11104-011-0770-6)
- Ebinger CJ, Keir D, Ayle A, Calais E, Wright TJ, Belachew M, Hammond JOS, Campbell E, Buck WR (2008) Capturing magma intrusion and faulting processes during continental rupture: seismicity of the Dabbahu (Afar) rift. *Geophys J Int* 174:1138–1152. doi:[10.1111/j.1365-246X.2008.03877.x](https://doi.org/10.1111/j.1365-246X.2008.03877.x)
- Fiala J, Vejnar Z (2004) The lithology, geochemistry, and metamorphic gradation of the crystalline basement of the Cheb (Eger) Tertiary Basin, Saxothuringian Unit. *Bull Geosci* 79:41–52
- Finizola A, Revil A, Rizzo E, Piscitelli S, Ricci T, Morin J, Angeletti B, Mocochain L, Sortini F (2006) Hydrogeological insights at Stromboli volcano (Italy) from geoelectrical, temperature, and CO_2 soil degassing investigations. *Geophys Res Lett*. doi:[10.1029/2006GL026842](https://doi.org/10.1029/2006GL026842)
- Finizola A, Aubert M, Revil A, Schütze C, Sortino F (2009) Importance of structural history in the summit area of Stromboli during the 2002–2003 eruptive crisis inferred from temperature, soil CO_2 , self-potential, and electrical resistivity tomography. *J Volcanol Geotherm Res* 183:213–227
- Finizola A, Ricci T, Deiana R, Cabusson SB, Rossi M, Praticelli N, Giocoli A, Romano G, Delcher E, Suski B, Revil A, Menny P, Gangi FD, Letort J, Peltier A, Villasante-Marcos V, Douillet G, Avard G, Lelli M (2010) Advective hydrothermal circulation on Stromboli volcano (Aeolian Islands, Italy) revealed by geophysical and geochemical approaches: implications for general fluid flow models on volcanoes. *J Volcanol Geotherm Res* 196:111–119. doi:[10.1016/j.jvolgeores.2010.07.022](https://doi.org/10.1016/j.jvolgeores.2010.07.022)
- Fischer T (2003) The August–December 2000 earthquake swarm in NW Bohemia: the first results based on automatic processing of seismograms. *J Geodyn* 35:59–81
- Fischer T, Horálek J (2003) Space–time distribution of earthquake swarms in the principal focal zone of the NW Bohemia/Vogtland seismoactive region: period 1985–2001. *J Geodyn* 35:125–144
- Fischer T, Michálek J (2008) Post 2000-swarm microearthquake activity in the principal focal zone of West Bohemia/Vogtland: space–time distribution and waveform similarity analysis. *Stud Geophys Geod* 52:493–511
- Fischer T, Štěpančíková P, Karousová M, Flechsig C, Gaballah M (2012) Imaging the Mariánské Lázně Fault (Czech Republic) by 3-D ground-penetrating radar and electric resistivity tomography. *Stud Geophys Geod* 56:1019–1036
- Fischer T, Horálek J, Hrbcová P, Vavryčuk V, Bräuer K, Kämpf H (2014) Intra-continental earthquake swarms in West Bohemia and Vogtland: a review. *Tectonophysics* 611:1–27. doi:[10.1016/j.tecto.2013.11.001](https://doi.org/10.1016/j.tecto.2013.11.001)
- Flechsig C, Bussert R, Rechner J, Schütze C, Kämpf H (2008) The Hartoušov Mofette field in the Cheb Basin, Western Eger Rift (Czech Republic): a comparative geoelectric, sedimentologic and soil gas study of a magmatic diffuse CO_2 -degassing structure. *Z Geol Wiss* 36(3):177–193
- Flechsig C, Fabig T, Rücker C, Schütze C (2010) Geoelectrical investigations in the Cheb Basin/W-Bohemia: an approach to

- evaluate the near-surface conductivity structure. *Stud Geophys Geod* 54:417–437
- Gautheron C, Moreira M, Allègre C (2005) He, Ne and Ar composition of the European lithospheric mantle. *Chem Geol* 217:97–112
- Geissler WH, Kämpf H, Kind R, Bräuer K, Klinge K, Plenefisch T, Horálek J, Zedník J, Nehyba V (2005) Seismic structure and location of a CO₂ source in the upper mantle of the western Eger (Ohre) rift. *Central Europe. Tectonics* 24:TC5001. doi:[10.1029/2004TC001672](https://doi.org/10.1029/2004TC001672)
- Gilbert RO (1987) Statistical methods for environmental pollution monitoring. Wiley, New York
- Girault F, Perrier F, Crockett R, Bhattacharai M, Koitala BP, France-Lanord C, Agrinier P, Ader M, Fluteau F, Gréau C, Moreira M (2014) The Syabru-Bensi hydrothermal system in central Nepal: 1. Characterization of carbon dioxide and radon fluxes. *J Geophys Res Solid Earth* 119:4017–4055. doi:[10.1002/2013JB010301](https://doi.org/10.1002/2013JB010301)
- Grünthal G (1989) About the history of earthquake activity in the focal region Vogtland/Western Bohemia. In: Bormann P (ed) Monitoring and analysis of the earthquake swarm 1985/86 in the region Vogtland/Western Bohemia. Akademie der Wissenschaften der DDR, Potsdam, pp 30–34
- Grünthal G, Schenk V, Zeman A, Schenková Z (1990) Seismotectonic model for the earthquake swarm of 1985–1986 in the vogtland/west bohemia focal area. *Tectonophysics* 174:369–383
- Günther T, Rücker C, Spitzer K (2006) Three dimensional modelling and inversion of dc resistivity data incorporating topography—II. Inversion. *Geophys J Int* 166(2):506–517
- Gürbüz A (2010) Geometric characteristics of pull-apart basins. *Lithosphere* 2(3):199–206
- Havíř J (2000) Stress analyses in the epicentral area of Nový Kostel (Western Bohemia). *Stud Geophys Geod* 44:522–536
- Hecht L, Vigneresse J, Morteani G (1997) Constraints on the origin of zonation of the granite complexes in the Fichtelgebirge (Germany and Czech Republic): evidence from a gravity and geochemical study. *Geol Rundsch* 86:S93–S109
- Hermann A, Kämpf H (2002) Seismicity in the central part of the Naab–Pritzwalk–Rostock lineament, related to mantle fluid activity? *EGS XXVII General Assembly*, Nice, 21–26 April 2002, abstract 5193
- Hermann A, Meier T, Jentzsch G, Ziegert A (2003) Similarity of waveforms and relative relocalisation of the earthquake swarm 1997/1998 near Werdau. *J Geodyn* 35:191–208
- Heuer B, Geissler WH, Kind R, Kämpf H (2006) Seismic evidence for asthenospheric updoming beneath the western Bohemian Massif, central Europe. *Geophys Res Lett* 33:L05311. doi:[10.1029/2005GL025158](https://doi.org/10.1029/2005GL025158)
- Heuer B, Geissler WH, Kind R, the BOHEMA working group (2011) Receiver function search for a baby plume in the mantle transition zone beneath the Bohemian Massif. *Geophys J Int* 187:577–594
- Hill DP, Prejean S (2005) Magmatic unrest beneath Mammoth Mountain, California. *J Volcanol Geotherm Res* 146:257–283
- Horálek J, Fischer T (2008) Role of crustal fluids in triggering the West Bohemia/Vogtland earthquake swarms: just what we know (a review). *Stud Geophys Geod* 52:455–478
- Horálek J, Fischer T (2010) Intraplate earthquake swarms in West Bohemia/Vogtland (Central Europe). *Jökull* 60:67–87
- Horálek J, Šílený J, Fischer T, Sláncová A, Boušková A (2000) Scenario of the January 1997 West Bohemia earthquake swarm. *Stud Geophys Geod* 44:491–521
- Hrubcová P, Geissler W (2009) The crust–mantle transition and the Moho beneath the Vogtland/West Bohemian region in the light of different seismic methods. *Stud Geophys Geod* 53:275–294
- Hrubcová P, Vavryčuk V, Boušková A, Horálek J (2013) Moho depth determination from waveforms of microearthquakes in the West Bohemia/Vogtland swarm area. *J Geophys Res* 118:1–17. doi:[10.1029/2012JB009360](https://doi.org/10.1029/2012JB009360)
- Hubatka F, Boušková A, Špičák A, Švancara J, Tilšarová R (2004) Ground penetrating radar profile measurements above the seismoactive area at the eastern margin of the Cheb Basin, Western Bohemia. *Geolines* 17:41–42
- Ibs-von Seht M, Blumenstein S, Wagner R, Hollnack D, Wohlenberg J (2001) Seismicity, seismotectonics and crustal structure of the southern Kenya rift-new data from the Lake Magadi Area. *Geophys J Int* 146:439–453
- Ibs-von Seht M, Plenefisch T, Klinge K (2008) Earthquake swarms in continental rifts—a comparison of selected cases in America, Africa and Europe. *Tectonophysics* 452:66–77
- Inguaggiato S, Calderone L, Inguaggiato C, Mazot A, Morici S, Vita F (2012) Long-time variation of soil CO₂ fluxes at the summit crater of Vulcano (Italy). *Bull Volcanol* 74:1859–1863
- Jakobsdóttir S, Roberts M, Gudmundsson G, Geirsson H, Slunga R (2008) Earthquake swarms at Upptyppningar, north-east Iceland: a sign of magma intrusion? *Stud Geophys Geod* 52:513–528
- Kämpf H, Bankwitz P (2005) The KTB deep crustal laboratory and the western Eger Graben. In: Koch R, Röhling HG (eds) *GeoErlangen 2005/Exkursionsführer, Schriftreihe der Deutschen Gesellschaft für Geowissenschaften* 40:37–108
- Kämpf H, Peterek A, Rohrmüller J, Kümpel HJ, Geissler WH (2005) The KTB deep crustal laboratory and the western Eger Graben. In: Koch R, Röhling HG (eds) *GeoErlangen 2005/Exkursionsführer, Schriftreihe der Deutschen Gesellschaft für Geowissenschaften* 40:37–108
- Kämpf H, Geissler WH, Bräuer K (2007) Combined gasgeochemical and receiver function studies of the Vogtland/NW Bohemia intraplate mantle degassing field. In: Christensen UR, Ritter JRR (eds) *Mantle plumes—a multidisciplinary approach*. Springer, Berlin
- Kämpf H, Bräuer K, Schumann J, Hahne K, Strauch G (2013) CO₂ discharge in an active, non-volcanic continental rift area (Czech Republic): characterisation (¹³C, ³He/⁴He) and quantification of diffuse and vent CO₂ emissions. *Chem Geol* 339:81–83
- Kárník V, Michal E, Molnár A (1957) Erdbebenkatalog der Tschechoslowakei bis zum Jahre 1956. *Travaux de l’Institut Géophysique de l’Académie Tchécoslovaque des Sciences* 69:411–598
- Key J, White RS, Soosalu H, Jakobsdóttir S (2011) Multiple melt injection along a spreading segment at Askja, Iceland. *Geophys Res Lett* 38:L05301. doi:[10.1029/2010GL046264](https://doi.org/10.1029/2010GL046264)
- Korn M, Funke S, Wendt S (2008) Seismicity and seismotectonics of West Saxony, Germany—new insights from recent seismicity observed with the Saxonian seismic network. *Stud Geophys Geod* 52:479–492
- Krüger JC, Romer RL, Kämpf H (2013) Late Cretaceous ultramafic lamprophyres and carbonatites from the Delitzsch Complex, Germany. *Chem Geol* 353:140–150
- Lewicki JL, Bergfeld D, Cardellini C, Chiodini G, Granieri D, Varley N, Werner C (2005) Comparative soil CO₂ flux measurements and geostatistical estimation methods on Masaya volcano, Nicaragua. *Bull Volcanol* 68:76–90
- Lewicki JL, Hilley GE, Dobeck L, Marino BDV (2012) Eddy covariance imaging of diffuse volcanic CO₂ emissions at Mammoth Mountain, CA, USA. *Bull Volcanol* 74:135–141
- Loseth H, Gading M, Wensaas L (2009) Hydrocarbon leakage interpreted on seismic data. *Mar Pet Geol* 26:1304–1319
- Malkovský M (1987) The Mesozoic and Tertiary basins of the Bohemian Massif and their evolution. *Tectonophysics* 137:31–42
- McClay K, Dooley T (1995) Analogue models of pull-apart basins. *Geology* 23(8):711–714

- Mlčoch B (2003) Character of the contact between the Saxothuringian and Teplá-Barrandian unit. *Geolines* 16:75
- Mlčoch B, Skácelová Z (2009) Digital elevation model of the crystalline basement of the Cheb and Sokolov Basin areas (Western Bohemia, Central Europe). *Z Geol Wiss* 37:145–152
- Mrlina J, Seidl M (2008) Relation of surface movements in West Bohemia to earthquake swarms. *Stud Geophys Geod* 52:549–566
- Mrlina J, Kämpf H, Kröner C, Mingram J, Stebich M, Brauer A, Geissler WH, Kallmeyer J, Matthes H, Seidl M (2009) Discovery of the first Quaternary maar in the Bohemian Massif, Central Europe, based on combined geophysical and geological surveys. *J Volcanol Geotherm Res* 182:97–112
- Neuhöfer H, Hemmann A (2005) Earthquake swarms in the Vogtland/Western Bohemian region: spatial distribution and magnitude–frequency distribution as an indication of the genesis of swarms? *J Geodyn* 39:361–385
- Nguyen F, Garambois S, Chardon D, Hermite D, Bellier O, Jongmans O (2007) Subsurface electrical imaging of anisotropic formations affected by a slow active reverse fault, Provence, France. *J Appl Geophys* 62(4):338–355
- Peterek A, Reuther CD, Schunk R (2011) Neotectonic evolution of the Cheb Basin (Northwestern Bohemia, Czech Republic) and its implications for the late Pliocene to Recent crustal deformation in the western part of the Eger Rift. *Z Geol Wiss* 5(6):335–365
- Pettinelli E, Beaubien SE, Lombardi S, Annan AP (2008) GPR, TDR, and geochemistry measurements above an active gas vent to study near-surface gas-migration pathways. *Geophysics* 73(1):11–15
- Pettinelli E, Beaubien SE, Zaja A, Menghini A, Praticelli N, Mattei E, Di Matteo A, Ciotoli G, Lombardi S (2010) Characterization of a CO₂ gas vent using various geophysical and geochemical methods. *Geophysics* 75(3):137–146
- Pfanz H, Vodník D, Wittmann C, Aschan G, Batic F, Turk B, Macek I (2007) Photosynthetic performance (CO₂-compensation point, carboxylation efficiency, and net photosynthesis) of timothy grass (*Phleum pratense* L.) is affected by elevated carbon dioxide in post-volcanic mofette areas. *Environ Exp Bot* 61:41–48
- Rennert T, Eusterhues K, Pfanz H, Totsche KU (2011) Influence of geogenic CO₂ on mineral and organic soil constituents on a mofette site in the NW Czech Republic. *Eur J Soil Sci* 62:572–580. doi:[10.1111/j.1365-2389.2011.01355.x](https://doi.org/10.1111/j.1365-2389.2011.01355.x)
- Revil A, Florsch N (2010) Determination of permeability from spectral induced polarization in granular media. *Geophys J Int* 181:1480–1498
- Revil A, Finizola A, Piscitelli S, Rizzo E, Ricci T, Crespy A, Angeletti B, Balasco M, Barde Cabusson S, Bennati L, Bolève A, Byrdina S, Carzaniga N, Di Gangi F, Morin J, Perrone A, Rossi M, Rouleau E, Suski B (2008) Inner structure of La Fossa di Vulcano (Vulcano Island, southern Tyrrhenian Sea, Italy) revealed by high resolution electric resistivity tomography coupled with self-potential, temperature, and soil CO₂ diffuse degassing measurements. *J Geophys Res* 113:B07207. doi:[10.1029/2007JB005394](https://doi.org/10.1029/2007JB005394)
- Revil A, Finizola A, Ricci T, Delcher E, Peltier A, Barde Cabusson S, Avard G, Baily T, Bennati L, Byrdina S, Cologne J, Di Gangi F, Douillet G, Lupi M, Letort J, Tsang Hin Sun E (2011) Hydrogeology of Stromboli volcano, Aeolian Islands (Italy) from the interpretation of resistivity tomograms, self-potential, soil temperature and soil CO₂ concentration measurements. *Geophys J Int* 186(3):88–98
- Rogie JD, Kerrick DM, Sorey ML, Chiodini G, Galloway DL (2001) Dynamics of carbon dioxide emission at Mammoth Mountain, California. *Earth Planet Sci Lett* 188:535–541
- Rojík P, Dašková J, Fejfar KJO, Kvaček Z, Pešek J, Sýkorová I, Teodoridis V (2010) Chebské panely. In: Pešek J (ed) Ložiska hnědého uhlí na území České republiky a jejich využití. Czech Geological Survey, Prague, pp 206–229
- Saito H, Goovaerts P (2000) Geostatistical interpolation of positively skewed and censored data in a dioxin-contaminated site. *Environ Sci Technol* 34:4228–4235
- Sakia RM (1992) The Box–Cox transformation technique: a review. *The Statistician* 41:169–178
- Sandig C, Sauer U, Bräuer K, Serfling U, Schütze C (2014) Comparative study of geophysical and soil-gas investigations at the Hartoušov (Czech Republic) natural CO₂ degassing site. *Environ Earth Sci* 72:1421–1434
- Saßmannshausen F (2010) Vegetationsökologische Charakterisierung terrestrischer Mofettenstandorte am Beispiel des west-tschechischen Plesná-Tals. PhD thesis, University Duisburg-Essen
- Sauer U, Schütze C, Leven C, Schlömer S, Dietrich P (2013) An integrative hierarchical monitoring approach for detecting and characterizing CO₂ releases. *Energy Proc* 37:4257–4267
- Schütze C, Sauer U, Beyer K, Lamert H, Bräuer K, Strauch G, Flechsig C, Kämpf H, Dietrich P (2012) Natural analogues: a potential approach for developing reliable monitoring methods to understand subsurface CO₂ migration processes. *Environ Earth Sci* 67:411–423
- Schütze C, Dietrich P, Sauer U (2013) Diagnostic monitoring to identify preferential near-surface structures for CO₂ degassing into the atmosphere: tools for investigations at different spatial scales validated at a natural analogue site. *Int J Greenh Gas Control* 18:285–295
- Špičáková A, Ulčný D, Koulidelková G (2000) Tectonosedimentary evolution of the Cheb Basin (NW Bohemia, Czech Republic) between Oligocene and Pliocene: a preliminary note. *Stud Geophys Geod* 44:556–580
- Suski B, Brocard G, Authemayou C, Muralles BC, Teyssier C, Holliger K (2010) Localization and characterization of an active fault in an urbanized area in central Guatemala by means of geoelectrical imaging. *Tectonophysics* 480:88–98
- Ulrych FC (2011) Recurrent Cenozoic volcanic activity in the Bohemian Massif (Czech Republic). *Lithos* 123:133–144
- Vavryčuk V (1993) Crustal anisotropy from local observations of shear-wave splitting in West Bohemia, Czech Republic. *Bull Seismol Soc Am* 83:1420–1441
- Vavryčuk V (2011) Principal earthquakes: theory and observations from the 2008 West Bohemia swarm. *Earth Planet Sci Lett* 305:290–296
- Vylita T, Žák K, Cílek V, Hercman H, Mikšíkova L (2007) Evolution of hot-spring travertine accumulation in Karlovy Vary/Carlsbad (Czech Republic) and its significance for the evolution of Tepla valley and Ohre/Eger rift. *Z Geomorphol N F* 51:427–442
- Weinlich FH, Tesař J, Weise SM, Bräuer K, Kämpf H (1998) Gas flux distribution in mineral springs and tectonic structure in northwest Bohemia. *J Czech Geol Soc* 43:91–110
- Weinlich FH, Bräuer K, Kämpf H, Strauch G, Tesař J, Weise SM (1999) An active subcontinental mantle volatile system in the western Eger rift, Central Europe: gas flux, isotopic (He, C, and N) and compositional fingerprints. *Geochim Cosmochim Acta* 63:3653–3671
- Weinlich FH, Bräuer K, Kämpf H, Strauch G, Tesař J, Weise SM (2003) Geochemie und Verteilung der Quellgase und tektonische Struktur des Eger-Rifts in der Oberpfalz und in Oberfranken, Bayern. *Zeit Deutschen Geol Gesell* 154:67–83
- Wendt J, Dietrich R (2003) Determination of recent crustal deformations based on precise GPS measurements in the Vogtland earthquake area. *J Geodyn* 35:235–246
- White RS, Drew J, Martens HR, Key J, Soosalu H, Jakobsdóttir S (2011) Dynamics of dyke intrusion in the mid-crust of Iceland. *Earth Planet Sci Lett* 304:300–312
- Wise DJ, Cassidy J, Locke CA (2003) Geophysical imaging of the Quaternary Wairoa North Fault, New Zealand: a case study. *J Appl Geophys* 53:1–16